

See discussions, stats, and author profiles for this publication at: <https://www.researchgate.net/publication/276293984>

Characterization of Fibrous Aggregated Morphologies and Other Complex Architectures Self-Assembled from Helical Alkyne and Triazole Polycarbodiimides (R)-and (S)-Families in the Bu...

ARTICLE *in* MACROMOLECULES · MAY 2015

Impact Factor: 5.8 · DOI: 10.1021/acs.macromol.5b00407

CITATIONS

2

READS

42

10 AUTHORS, INCLUDING:



Dumindika Siriwardane

University of Texas at Dallas

9 PUBLICATIONS 10 CITATIONS

[SEE PROFILE](#)



James F Reuther

University of Texas at Austin

9 PUBLICATIONS 50 CITATIONS

[SEE PROFILE](#)



Sergei S. Sheiko

University of North Carolina at Chapel Hill

168 PUBLICATIONS 7,657 CITATIONS

[SEE PROFILE](#)



Bruce Novak

University of Texas at Dallas

135 PUBLICATIONS 5,654 CITATIONS

[SEE PROFILE](#)

Characterization of Fibrous Aggregated Morphologies and Other Complex Architectures Self-Assembled from Helical Alkyne and Triazole Polycarbodiimides (*R*)- and (*S*)-Families in the Bulk and Thin Film

Oleg V. Kulikov,^{*,†} Dumindika A. Siriwardane,[†] James F. Reuther,[‡] Gregory T. McCandless,[†] Hao-Jan Sun,[§] Yuanchao Li,^{||} Samsuddin F. Mahmood,[†] Sergei S. Sheiko,^{||} Virgil Percec,[§] and Bruce M. Novak^{*,†}

[†]Department of Chemistry, University of Texas at Dallas, Richardson, Texas 75080, United States

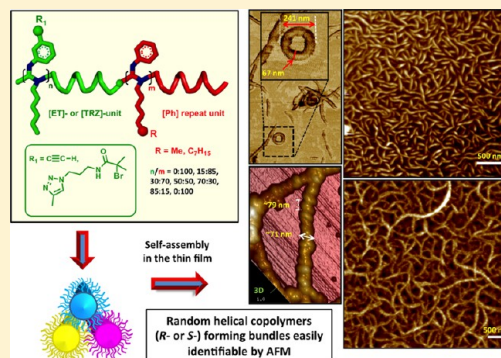
[‡]Department of Chemistry, University of Texas at Austin, Austin, Texas 78712, United States

[§]Department of Chemistry, University of Pennsylvania, Philadelphia, Pennsylvania 19104, United States

^{||}Department of Chemistry, The University at North Carolina at Chapel Hill, Chapel Hill, North Carolina 27599, United States

Supporting Information

ABSTRACT: We report here the self-assembly studies of 22 polycarbodiimides (PCDs) in complex morphologies such as fibers, looped fibers, fibrous networks, ribbons, worm-like aggregates, toroidal structures, and craters that were examined by combination of TMAFM, TEM, SEM, and powder XRD methods as well as semiempirical modeling. Morphology characterization in the thin film (TMAFM, TEM) and in bulk (SEM, pXRD) revealed the formation of fiber-like aggregates assembled from the bundles of individual helices. In certain cases superhelical motifs of both right- and left-handed screw senses were identified. It seemed likely that the great variety of morphologies observed is a result of extensive hydrophobic side chain/side chain interactions of the singular polycarbodiimide strands.



INTRODUCTION

Over the years there has been a considerable interest in designing, constructing, and testing different classes of functional helical systems¹ driven by the wide range of their potential applications such as asymmetric organocatalysis,^{2,3} switchable chromatographic enantioseparation,⁴ and electrical switching of molecular wires.⁵ So far, a large variety of structurally diverse helical systems have been explored. Thus, Huc et al. reported the synthesis of aromatic oligoamide helical foldamers,^{6–10} branched foldamers,¹¹ helical molecular capsules,^{12,13} and double-helix architectures.¹⁴ Because of their synthetic accessibility, polyacetylenes (especially phenylacetylenes) would probably remain one of the most popular scaffolds in the toolbox of polymer chemist investigating helicity. To date, a number of different polyacetylenes¹⁵ have been investigated, including dynamic helical poly(phenylacetylene)s,^{16,17} poly(*p*-*n*-hexyloxyphenylacetylene)s,¹⁸ and dendronized polyphenylacetylenes.¹⁹ Helical structures found to be preferred conformation for the numerous types of polyisocyanates.^{20,21} Extensive studies have been undertaken on poly(*n*-butyl isocyanate), PBIC,²² poly(*n*-hexyl isocyanate), PHIC,^{23–27} poly(phenylpropyl isocyanate),²⁸ and poly(phenyl isocyanate)²⁹ showing high potential in the areas of chiral

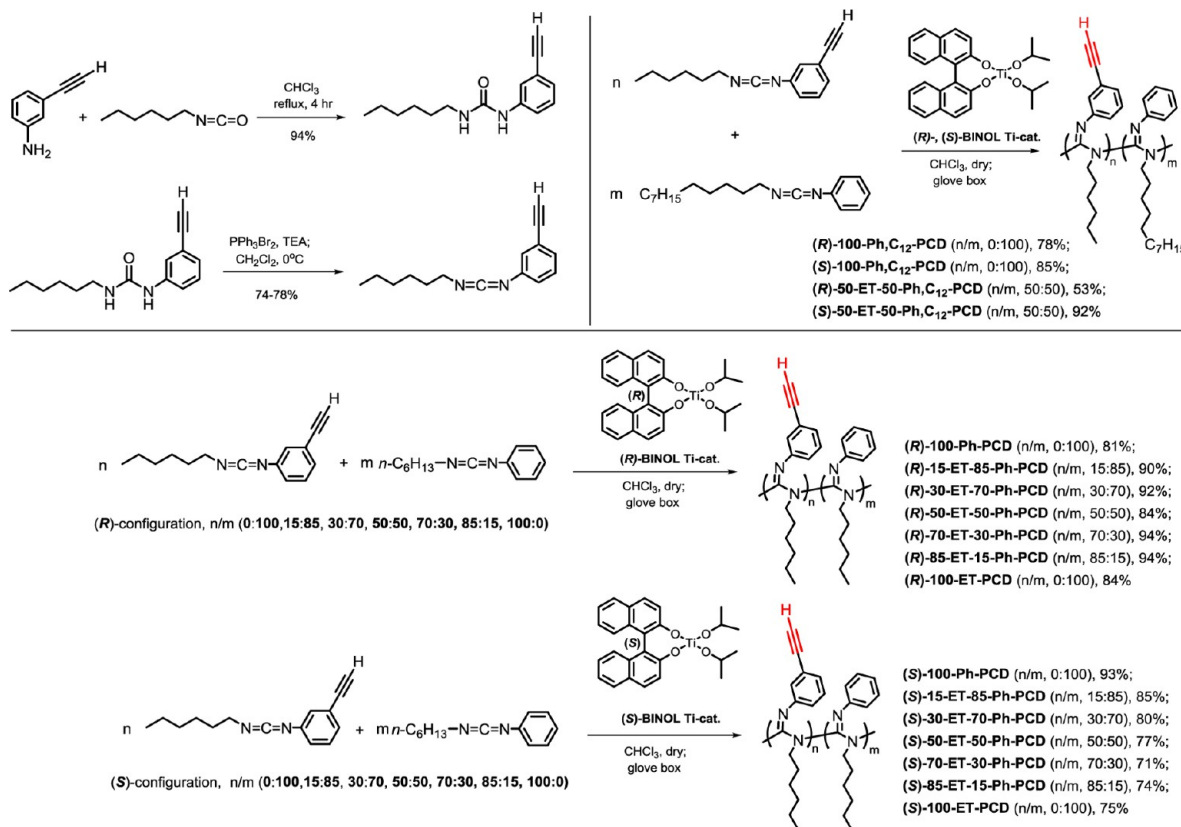
recognition, chiroptical switching, and design of liquid crystalline materials.^{30–32} In addition to that, macromolecules having different helical scaffolds such as amphiphilic poly(*m*-phenylene ethynylene)s,³³ polyisocyanides,³⁴ riboflavin-containing polymers,³ polyallenes,³⁵ and chiral polycarbodiimides^{36,37} have attracted considerable attention.

In 1994, Goodwin and Novak discovered the controlled polymerization of carbodiimide monomers with titanium initiator³⁸ leading to inherently helical polycarbodiimide scaffold. Helical polycarbodiimides (or polyguanidines) have shown many remarkable properties (chiral orienting media,³⁹ thermo-controllable optical switching,⁴⁰ chiroptical switching,^{41–43} liquid crystalline properties,^{44,45} and antibacterial activity⁴⁶). Tunable self-assembly of the rod-coil block copolymers has been well documented with regard to their photophysical properties as well as optoelectronic and stimuli-responsive applications.^{47–51} Recently, we described the synthesis and self-assembly studies of rod-coil graft copolymer consisting of poly(4-bromostyrene) chain and polycarbodiimides^{36,37} showing high potential in the areas of chiral

Received: February 25, 2015

Revised: April 28, 2015



Scheme 1. Synthesis of *N*-3-Ethynylphenyl-*N'*-hexylcarbodiimide and All Alkyne PCDs

mide rigid rod.⁵² Inspection of its thin film morphology revealed nanofibular aggregation behavior with nanofibril average diameter \sim 171 nm. This fibrillar morphology appears to be typical for conjugated block copolymers or oligomers.^{53,54} In this work, to unequivocally clarify the role and function of the polycarbodiimide scaffold in fibrils self-assembly, we performed AFM measurements on a series of (*R*)- and (*S*)-polycarbodiimides. Current studies represent a logical extension of our earlier efforts on the synthesis of optically active alkyne polycarbodiimides bearing one or two modifiable alkyne moieties per repeat unit.^{55,56}

Here, we report the synthesis and systematic self-assembly studies of (*R*)- and (*S*)-families of helical rigid-rod alkyne and triazole polycarbodiimides derived from carbodiimide monomers by using titanium(IV) (*R*)- and (*S*)-BINOL catalyst. We surmise that these macromolecular entities can act as simplified models of tunable self-assembly in thin film leading to the detailed understanding of underlying mechanism of self-organization into fibrillar aggregates. Also, postmodification of unprotected ethynyl groups by click protocol offers an opportunity to functionalize further these protein-like macromolecules.

RESULTS AND DISCUSSION

Synthesis of Ethynyl- and Triazole-Polycarbodiimides (PCDs). The synthesis of molecules in these two series (*R*- and *S*-) of ethynylpolycarbodiimides has been accomplished through the standard coordination–insertion polymerization of the carbodiimide monomers using titanium(IV) catalyst at room temperature under an inert atmosphere.⁵⁵ Altering the ratio of carbodiimide precursors, phenyl hexylcarbodiimide monomer (denoted Ph) and its 3-ethynyl analogue (ET),

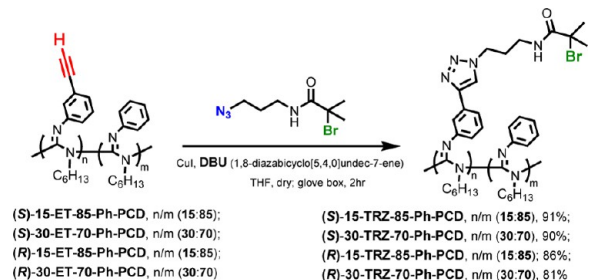
allowed us to generate two families of alkyne-functionalized polymers with repeat unit compositions varying in the ranges 0:100 (100-Ph), 15:85 (15-ET-85-Ph), 30:70 (30-ET-70-Ph), 50:50 (50-ET-50-Ph), 70:30 (70-ET-30-Ph), 85:15 (85-ET-15-Ph), and 100:0 (100-ET). The carbodiimide monomers were obtained in good to excellent yields from the corresponding ureas (Scheme 1). Further CuAAC “click” chemistry functionalization of selected (*R*)- and (*S*)-polycarbodiimides afforded their triazole derivatives in almost quantitative yield (Scheme 2). Both (*R*)- and (*S*)-families compositions having low *n/m* ratio, e.g., 15-ET-85-Ph and 30-ET-70-Ph, were selected for “click” coupling with *N*-(3-azidopropyl)-2-bromo-2-methylpropane amide due to the solubility concern of the resulting triazole derivatives. Alkyne compositions with higher *n/m* ratio tend to produce completely insoluble (or having very limited solubility in organic solvents) materials during the course of Cu(I)-catalyzed “click” synthesis, possibly as a result of cross-linking side reaction. Though oxygen-free atmosphere was used to conduct “click” protocol, we hypothesize that well-known Glaser coupling may occur in a system with unprotected ethynyl groups in the presence of Cu(I) halides. In furthering our goal of constructing helical rod-like copolymers and functional materials thereof, triazole PCDs bearing a Br-terminated moiety might be employed as ATRP initiators in copolymerization with styrene (not presented in the current work).

All newly synthesized polymers were characterized by ¹H NMR, ¹³C NMR, and FTIR (Figures S37–S65). Size exclusion chromatography (SEC) performed on these polymers using polystyrene standards determined the relative molecular weight: (*R*)-15-TRZ-85-Ph-PCD ($M_n = 9063$ Da, PDI = 3.57), (*S*)-15-TRZ-85-Ph-PCD ($M_n = 10\,780$ Da, PDI = 3.61),

and (*R*)-30-TRZ-70-Ph-PCD ($M_n = 9050$ Da, PDI = 1.82). In general, solvent used as eluent effects on resulting M_n and PDI values that could be attributed to the solubility changes and/or different adhesion of PCDs to the stationary phase. For instance, (*R*)-30-ET-70-Ph-PCD displayed different M_n numbers depending on solvent system used ($M_n = 10\,041$ Da, PDI = 2.61, CHCl_3 ; $M_n = 12\,429$ Da, PDI = 3.13, THF; $M_n = 14\,617$ Da, PDI = 1.58, DMF). As it was reported earlier,⁵² accurate molecular weight and PDI values determination for different classes of polycarbodiimides seem to be challenging due to the strong affinity of their nitrogen-rich, rigid-rod structures to SEC column matrix materials. Data on (*S*)- and (*R*)-families of alkyne PCDs are summarized in Table S1.

Helical polycarbodiimides are known to be intrinsically chiral.³⁷

Scheme 2. Synthesis of the Triazole-PCDs via “Click” Protocol



As expected, the resulting alkyne random copolymers demonstrated positive or negative relative optical rotation values depending on what enantiomer (*R*- or *S*-) of titanium(IV) BINOL catalyst was used to mediate polymerization. We assume that (*R*)-enantiomer induced the formation of right-handed *P*-helix (+) while (*S*)-enantiomer gives left-handed *M*-helix (-). This is consistent with experimentally determined signs of specific optical rotation for both alkyne polycarbodiimide families (Table S2). All polymer products were purified by precipitation in MeOH containing ~1% (v/v) of DBU (1,8-diazabicyclo[2.5.0]undec-7-ene) to remove either residual Ti(IV)-BINOL catalyst or Cu^{2+} (after “click” coupling). Characterization of the purified “click” products by ^1H NMR showed the disappearance of strong peak at ~2.9 ppm attributed to the terminal alkyne proton (Figures S52–S55). Also, successful click reaction may be verified through visualization of the triazole moiety proton at ~8 ppm.⁵⁷ Furthermore, FTIR analysis was indicative of substantial alkyne conversion, demonstrating significant decrease of strong stretching band at ~3307 cm^{-1} that corresponds to the terminal ethynyl group (Figures S64 and S65). It is unclear from the FTIR standpoint if “alkyne-to-triazole” conversion was fully completed within 2 h “click” coupling; nevertheless, longer reaction times should be avoided since material in reaction vessel is prone to form green insoluble gel.

Thin-Film Morphologies of PCDs Examined by AFM. The thin film morphologies have been prepared by either spin-coating or by the drop-cast method of CHCl_3 solutions of polycarbodiimides (*R*- and (*S*)-families on different substrates including mica, silicon wafer, and HOPG (highly ordered pyrolytic graphite). Chloroform was our solvent of choice for these aggregation studies since its ability to dissolve easily all ethynyl-PCDs as well as their respective triazole derivatives.

Also, there have been reports from the Stefan lab showing successful use of this solvent for AFM characterization of polythiophene-based fibrillar morphologies.^{58–64} Inspection by tapping mode AFM revealed different types of elongated networks (Figures 1–9 and Figures S1–S31) depending on concentration of the stock solution, solvent of choice, deposition method, and the structure of polycarbodiimide (e.g., alkyne vs triazole derivatives, C_6 -side chains vs elongated C_{12} -chains, ratio between ethynyl- C_6H_4 and Ph fragments).

Figure 1 phase (panels a and c) and height (panel b) diagrams showed densely packed curly shaped morphologies obtained from (*S*)-15-TRZ-85-Ph-PCD when spin-coated from CHCl_3 solution onto silicon wafer. The dimensions of fibers formed range from ~25 to ~43 nm. When the same (*S*)-15-TRZ-85-Ph-PCD composition was prepared via the drop-cast method, thin fibers ($d \sim 15$ nm, Figure 1, panel d; Figure S1) and ribbons ($d \sim 30\text{--}50$ nm, Figure 1, panels e and f; Figures S2 and S3) were observed as predominant morphologies implying that both deposition method and concentration of stock solution likely play a significant role in self-assembly process and determine the shape and size of resulting aggregates. One can assume that spin-coating would give more uniform surface throughout the film than the drop-cast method. However, direct observation of individual fibers having diameter lesser than 20 nm seems to be problematic by both techniques, and the best results were obtained when dilute (0.079 mg/mL) solution was drop-cast on silicon wafer (panel d) and thermally annealed at 76 °C for 12 h.

The role of thermal annealing in the fiber formation is not quite clear. It is believed that thermal annealing allows aggregates to reach thermodynamic equilibrium. Annealed sample shown in the panel d of Figure 1 demonstrated mixed morphologies including long (occasionally, looped) fibers, short fibers, and amorphous aggregates. The presence of interesting worm-like aggregates is apparent in panels e, f (Figure 1), and a–d (Figure S3). Similarly looking ribbon motifs (separated or assembled into networks) could be easily identified in Figure S2 displaying morphologies after thermal annealing at 76 °C that provides evidence for thermodynamic stability of these elongated supramolecular constructs. Choice of the substrate used for the sample deposition appears to be critical for successful visualization; therefore, we spin-coated selected alkyne and triazole PCDs on mica and highly ordered pyrolytic graphite (HOPG) hoping to obtain more accurate measurement results and, possibly, image singular helical polymer chains. The micrographs shown in panels a–f of Figure 2 and Figure S6 (panels a–c) demonstrated the range of fiber-like aggregates observed for (*S*)-15-TRZ-85-Ph-, (*R*)-15-TRZ-85-Ph-, and (*R*)-30-TRZ-70-Ph-PCDs.

We hypothesize that using very low concentration of the stock solution (5×10^{-5} mg/mL, Figure 2e) prevents the extensive crystallization of the adjacent polymer chains with one another to form a network that otherwise could be clearly seen in panels b and f of Figure 2. Panel d shows sharp angles and straight polymer chains that are not uncommon for AFM images taken on HOPG substrate.⁶⁵ This is believed due to epitaxial alignment of singular polymer chains on the graphite surface.

Figures S8 and S9 summarize the AFM characterization data on (*R*)- and (*S*)-30-TRZ-70-Ph-PCDs spin-coated from CHCl_3 either onto mica or Si-wafer that provides sufficient evidence for dense packing of polymer molecules at moderate concentrations (0.625, 1.25, and 2.5 mg/mL).

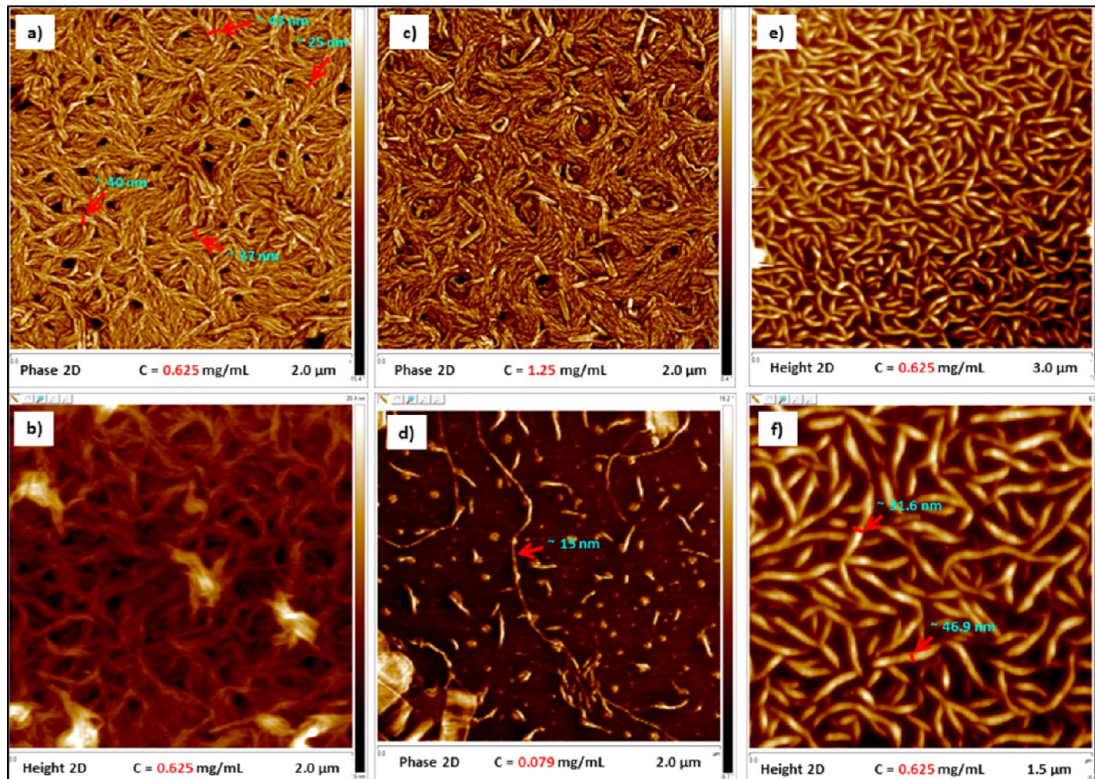


Figure 1. Phase AFM micrographs of (S)-15-TRZ-85-Ph-PCD. Spin-coated from chloroform (panels a–c); drop-cast (panels d–f). Scan size = $2.0 \times 2.0 \mu\text{m}$ (panels a–d); $3.0 \times 3.0 \mu\text{m}$ (panel e); $1.5 \times 1.5 \mu\text{m}$ (panel f). Sample d was annealed at 76°C overnight; samples a, b, c, e, and f were inspected without prior thermal annealing.

In order to elucidate the effect of different composition on morphologies visualized by AFM, we tested a number of alkyne PCDs having the different ratio of arylalkyne (ET) and phenyl (Ph) components (Figures 3–7 and Figures S10–S23). As anticipated, alkyne PCDs derived from (R)- and (S)-families exhibited unremarkable difference in aggregation behavior.

Figure 3 and Figure S14 demonstrate fibrillar aggregates assembled from (S)-85-ET-15-Ph-PCD prior to thermal annealing (Figure 3, panel a) and annealed at 80°C samples (Figure 3, panels b, c). Remarkably, short fibers shown in Figure 3c display more order and appear to be oriented in one direction, while tangled morphologies in panels a and b are randomly oriented covering the area of specimen. In general, thermal annealing has no or insignificant effect on ordering of morphologies that is indicative of thermodynamic stability of aggregates derived from PCDs.

Very long entangled fibers ($>5 \mu\text{m}$) with diameter $\sim 80 \text{ nm}$ were detected in the lower row panels d–f of Figure 3 showing AFM micrographs of (S)-100-ET-PCD (more details on aggregation behavior of this composition at different concentrations could be found in Figures S15 and S16).

We have found that formation of entangled well-resolved fibers is a common trend for alkyne compositions having high content of ethynyl-containing residue. Along with above-mentioned (S)-85-ET-15-Ph-PCD and (S)-100-ET-PCD, other “alkyne-rich” compositions such as (S)-70-ET-30-Ph- (Figure 4) and (S)-50-ET-50-Ph-PCD (Figure 5) are prone to self-assemble into interconnected fibrous morphologies. Selected AFM micrographs of (S)-70-ET-30-Ph-PCD presented in panels of Figure 4 showed aggregates $\sim 100\text{--}150 \text{ nm}$ in width and $\sim 5 \mu\text{m}$ in length (additional images could be found in Figure S17). Notably, unlike other alkyne

compositions with low alkyne content that showed significantly better quality AFM images in phase diagrams rather than their respective almost featureless height profiles, (S)-70-ET-30-Ph-PCD AFM height representations provided excellent contrast and detailed visualization of morphologies observed. We believe that exceptional ability of high ($n/m \geq 50$) ratio compositions to make distinct fibers may be resulted from the decrease in their solubility that induces polymer macromolecules to crystallize with one another forming discrete fibrillar aggregates.

Figure 5 (panels a and b, composition (S)-50-ET-50-Ph-PCD) showed very dense, possibly, lamellar type packing of fibrous morphologies with an average width roughly estimated $\sim 45 \text{ nm}$ (panel b). A close inspection of these aggregates in higher magnification mode (panel b) revealed wave-like lamellar ordering. It is clearly seen that polymer rods within domain areas are aligned and have preferential orientations. Lower concentrations of this composition are shown in Figure S18. In general, the use of concentration as high as 30 mg/mL is not typical for AFM morphological determinations and likely represents upper practical limit for one whose goal is to detect separate individual fibers and, moreover, microscope discrete polymer macromolecules.

Distinct separate fibers varying in width from ~ 18 to 30 nm could be clearly seen in panel c of Figure 5 for (S)-15-ET-85-Ph-PCD that is common observation for concentrations of such a low value (0.157 mg/mL). These discoveries are consistent with results obtained by using HOPG as a substrate (Figure S19). More images of this composition are shown in Figure S20. Testing the (S, R)-100-Ph-PCD obtained from *N*-phenyl-*N'*-hexylcarbodiimide monomer with no use of catalyst showed unremarkable differences in aggregation behavior comparatively to its optically active (R)- and (S)-analogues (Figures S21–

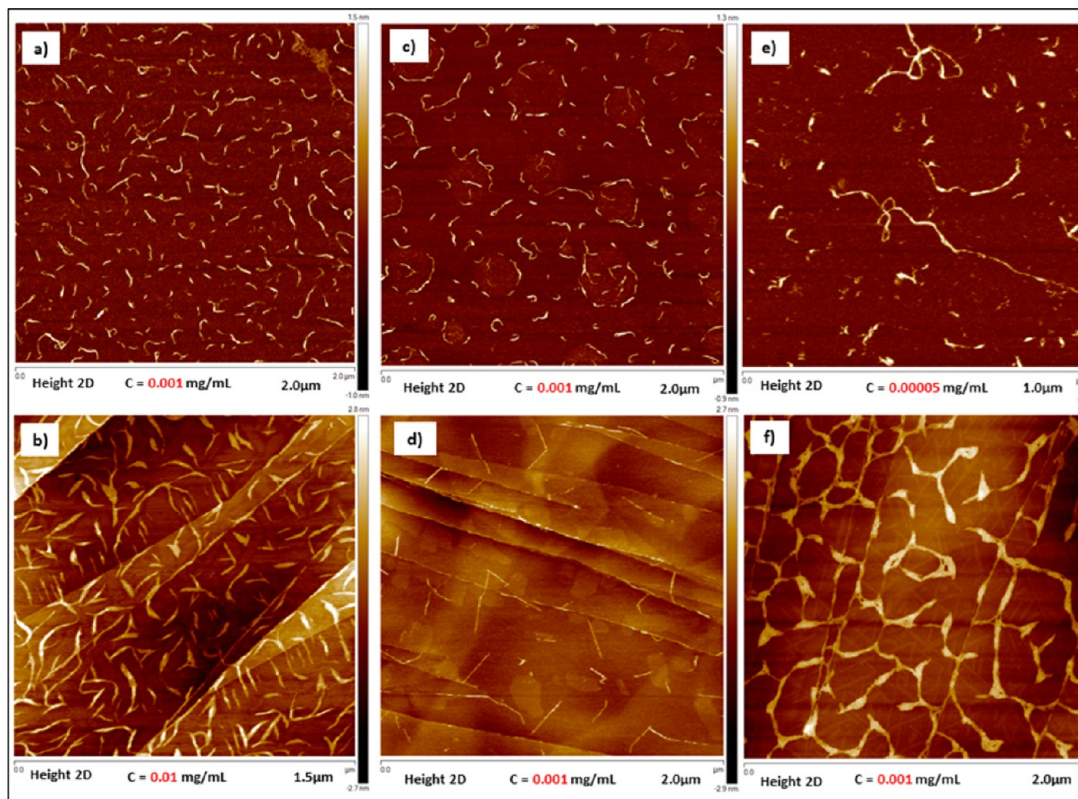


Figure 2. Phase AFM micrographs of (*S*)-15-TRZ-85-Ph- (panels a, b), (*R*)-15-TRZ-85-Ph- (panels c, d), and (*R*)-30-TRZ-70-Ph-PCDs (panels e, f) spin-coated from chloroform onto mica (panels a, c, e) and HOPG (panels b, d, f). Scan size = 2.0 × 2.0 μm (panels a, c, d, f); 1.5 × 1.5 μm (panel b); 1.0 × 1.0 μm (panel e).

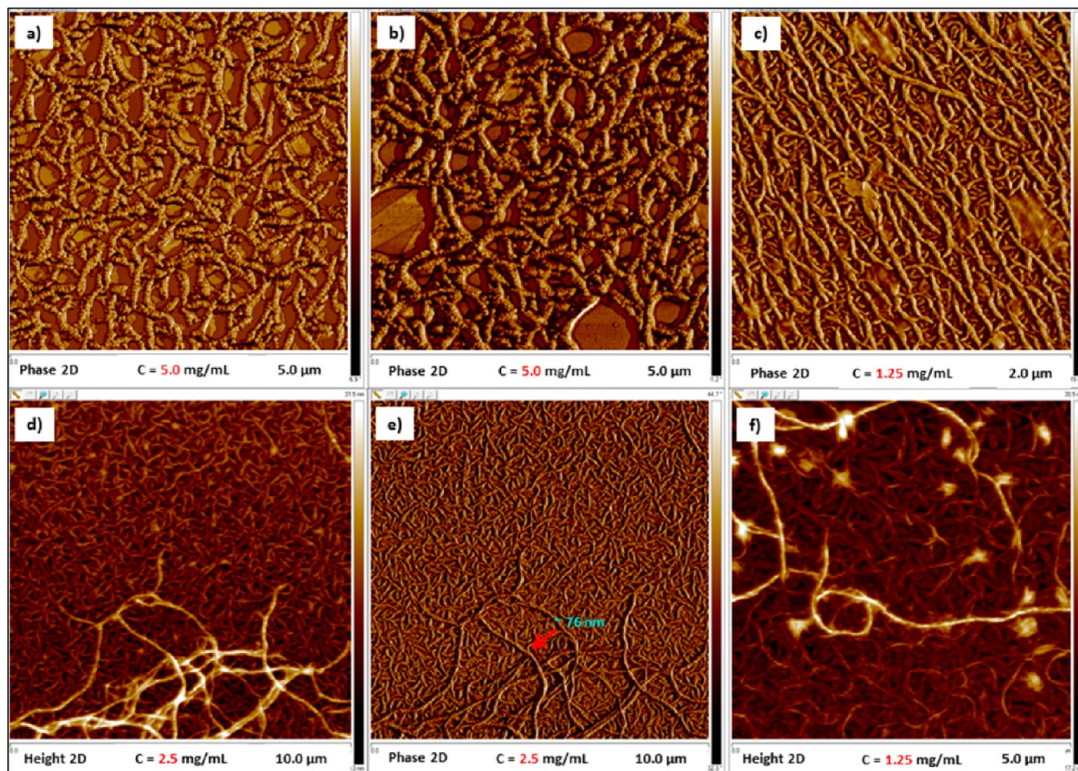


Figure 3. Selected phase and height AFM micrographs of (*S*)-85-ET-15-Ph-PCD obtained by spin-coating from CHCl₃ before thermal annealing (panel a) and after annealing (panels b, c); (*S*)-100-ET-PCD (panels d–f) spin-coated from CHCl₃. Scan size = 5.0 × 5.0 μm (panels a, b, f); 2.0 × 2.0 μm (panel c); 10.0 × 10.0 μm (panels d, e).

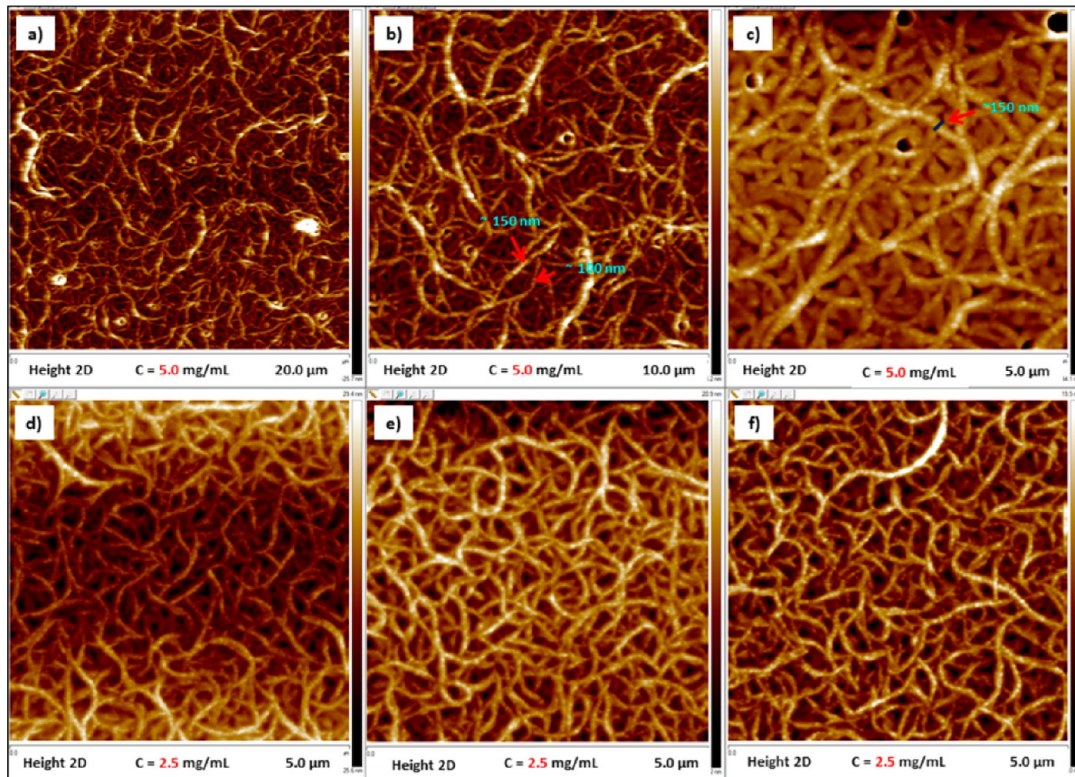


Figure 4. Height AFM micrographs of (S)-70-ET-30-Ph-PCD obtained by spin-coating from CHCl_3 . Scan size = $20.0 \times 20.0 \mu\text{m}$ (a); $10.0 \times 10.0 \mu\text{m}$ (b); $5.0 \times 5.0 \mu\text{m}$ (c–f).

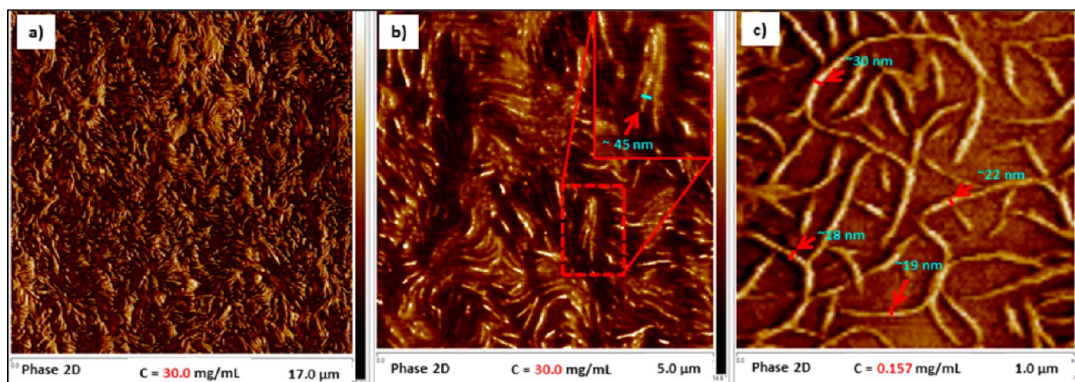


Figure 5. Phase AFM micrographs of (S)-50-ET-50-Ph-PCD obtained by drop-cast from CHCl_3 on Si-wafer (panels a, b); (S)-15-ET-85-Ph-PCD spin-coated from CHCl_3 on Si-wafer (panel c). Scan size = $17.0 \times 17.0 \mu\text{m}$ (panel a); $5.0 \times 5.0 \mu\text{m}$ (panel b); $1.0 \times 1.0 \mu\text{m}$ (panel c).

S23). To elucidate the effect of long aliphatic chains on morphological behaviors, we inspected some model compounds bearing long dodecyl side chains attached to polycarbodiimide backbone. Insignificant morphological differences observed for C_{12} -PCDs, if compared with their respective C_6 -analogues, arise from their structural differences. We assume that longer aliphatic chains (C_{12} - vs C_6 -) having increased conformational flexibility are prone to interdigitate more efficiently that seems to be important for successful crystallizing of neighboring macromolecules and formation of network patterns/fibrillar motifs clearly identifiable in Figures S22(2–5).

The difference between (R)- and (S)-families of alkyne PCDs in their ability to self-organize into elongated fibrous aggregates is unnoticeable. Figure 6 shows AFM phase images of (R)-50-ET-50-Ph-PCD and (R)-70-ET-30-Ph-PCD spin-coated from

CHCl_3 onto Si-wafer that are typical in appearance. The presence of fiber-like aggregates is apparent for both compositions, and as anticipated, low concentrations ($C = 0.625 \text{ mg/mL}$) promoted fiber separation (Figure 6c).

Interestingly, (R)-70-ET-30-Ph-PCD displayed highly ordered supramolecular organizations (Figure 6b and Figure S23a), whereas (R)-50-ET-50-Ph- (Figure 6a), (R)-30-ET-70-Ph- (Figure S23c), and (R)-100-Ph-PCDs (Figure S23e,f) demonstrated less ordered fibrillar aggregates at the same concentration value ($C = 1.25 \text{ mg/mL}$). However, it appears that such insignificant changes may likely result from fluctuations in concentration or be thermally driven during sample preparation rather than arose from actual structural differences between compositions tested. More images of R-series (R-100-ET-, R-50-ET-50-Ph-, and R-85-ET-15-Ph-PCDs) are given in the Supporting Information (Figure S23-2).

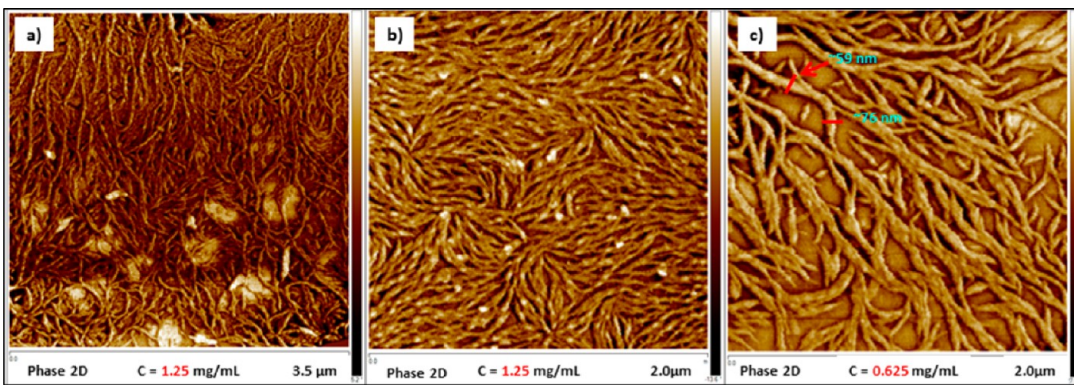


Figure 6. Phase AFM micrographs of (R)-50-ET-50-Ph-PCD obtained by spin-coating from CHCl_3 on Si-wafer (panel a); (R)-70-ET-30-Ph-PCD spin-coated from CHCl_3 on Si-wafer (panels b, c). Scan size = $3.5 \times 3.5 \mu\text{m}$ (panel a); $2.0 \times 2.0 \mu\text{m}$ (panels b, c).

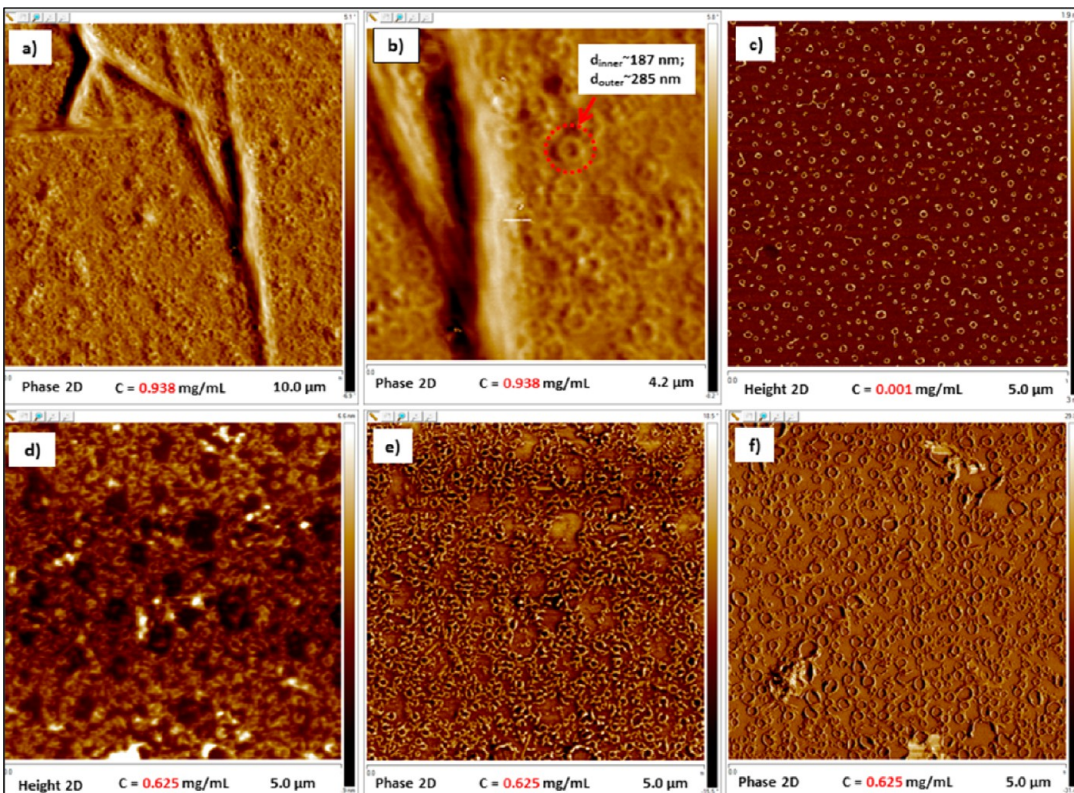


Figure 7. AFM micrographs of (S)-30-TRZ-70-Ph-PCD obtained by drop-cast from 1,2,4-trichlorobenzene on Si-wafer (panels a, b), (R)-50-ET-50-Ph-PCD spin-coated from CHCl_3 on mica (panel c), and (S)-50-ET-50-Ph-PCD spin-coated from CHCl_3 on Si-wafer (panels d–f). Scan size = $10.0 \times 10.0 \mu\text{m}$ (panel a); $5.0 \times 5.0 \mu\text{m}$ (panels c–f); $4.2 \times 4.2 \mu\text{m}$ (panel b).

Undoubtedly, one of the most intriguing aspects of PCDs is their ability to self-assemble into doughnut-like architectures. This unusual behavior was observed for some alkyne as well as triazole families regardless of deposition method and solvent used for the sample preparation, probably, as a result of higher order aggregates formation. Figure 7 (panels a and b) displayed small toroidal aggregates assembled from (S)-30-TRZ-70-Ph-PCD drop-cast from 1,2,4-trichlorobenzene onto Si-wafer. A closer inspection (Figure 7b and Figure S24b–f) revealed macromolecular toroids with inner diameter $\sim 187 \text{ nm}$, whereas their outer diameter is estimated $\sim 285 \text{ nm}$ (at least, for one of these species that was visualized more distinctively than others).

Appreciably greater nanorings were detected (Figure S22-2i–k, S22-4f, S22-5g) for long-chained PCDs bearing a dodecyl substituent.

At this point the exact nature of this phenomenon is not fully understood, and therefore, more systematic studies are needed. We speculate that individual fibers could interact with one another forming supramolecular bundles and, eventually, highly ordered lamellar structures discussed above (Figure 5a,b). Another possibility is to form enclosed aggregates when termini of bent fibers are in close proximity and could eventually fuse together yielding looped assemblies. This proposed mechanism is somewhat similar to reported earlier aggregation of twisted cylindrical micelles into super-rings⁶⁶ or cylinder collapse to toroidal micelle structures discovered by Pochan and Wooley.⁶⁷ An alternative explanation is that the small spherical droplets of

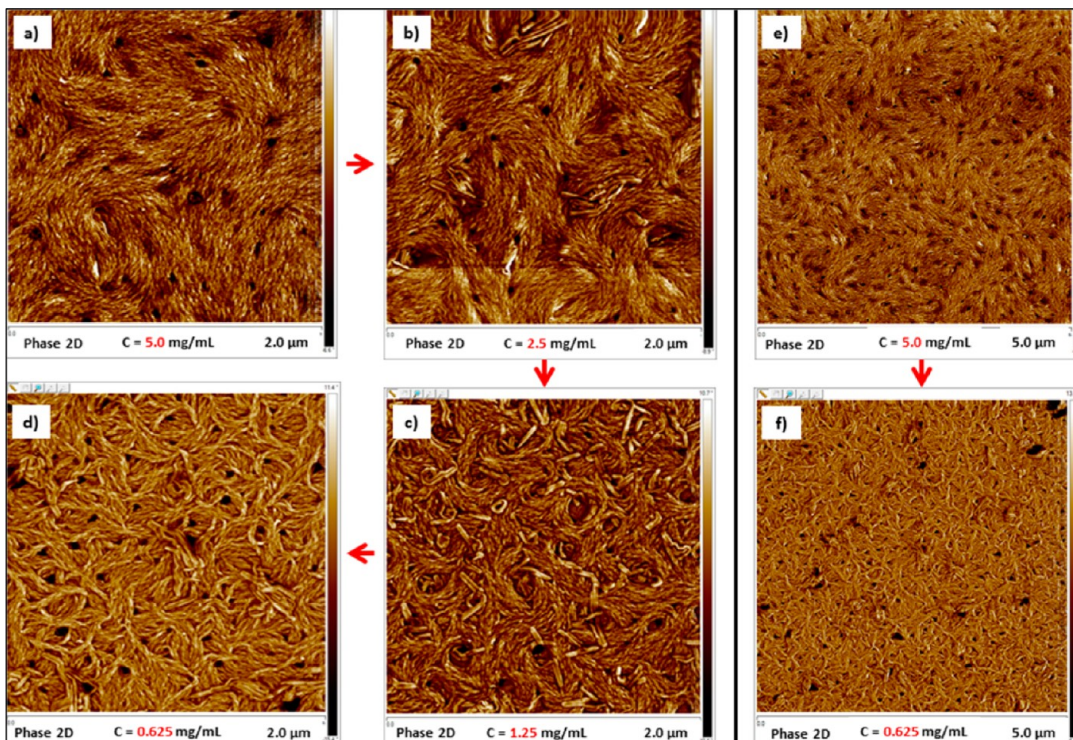


Figure 8. Phase AFM micrographs of (S)-100-ET-PCD thin film. Morphological changes observed at dilution of CHCl_3 stock solutions: 5.0 mg/mL (panel a); 2.5 mg/mL (panel b); 1.25 mg/mL (panel c); 0.625 mg/mL (panel d); 0.313 mg/mL (panel e); 0.157 mg/mL (panel f). Scan size = $5.0 \times 5.0 \mu\text{m}$.

highly concentrated polymer solution formed on the Si-wafer surface due to dewetting occurred as a result of solvent evaporation during sample deposition may further collapse into the small doughnuts or craters. Dewetting of thin polymer films that may control morphology of the polymeric nanostructures resulting on a solid support such as Si-wafer⁶⁸ or glass slide surface⁶⁹ is well-known phenomenon when failure of a liquid coating to remain continuous on a substrate⁷⁰ yielded wrinkly pattern. Nature may combine both proposed mechanisms in order to generate these unusual ring-shaped supramolecular constructs. Toroidal architectures shown in panels c–f (Figure 7) are assembled from (R)-50-ET-50-Ph- and (S)-50-ET-50-Ph-PCDs when spin-coated from CHCl_3 solution onto mica (panel c, $C = 1 \times 10^{-3}$ mg/mL) and Si-wafer (panels d–f, $C = 0.625$ mg/mL). More detailed images of toroidal architectures are displayed in Supporting Information (Figures S24 and S25). In summary, regardless of deposition method (drop-cast vs spin-coating), solvent of choice, type of substrate used for deposition (mica vs Si-wafer), and concentration ranging from 1×10^{-3} to 5.0 mg/mL, alkyne and triazole PCDs of different composition having either (R)- or (S)-configuration of their amidine backbone may be occasionally organized into toroid-shaped aggregates as a result of thin film rupture and dewetting processes. Assuming instability of such kind of aggregates,⁷¹ one can infer that further rearrangement into the other preferential morphologies is likely, especially during thermal annealing.

AFM Concentration Series. To investigate the role of concentration in the formation of certain types of aggregates, extensive series of solutions have been prepared and examined by AFM (Figure 8). Despite the fact that there is no linear relationship between concentration and the diameter of fibers/ribbons formed when spin-coated from CHCl_3 on Si-wafer, it

seemed that decreasing the concentration of stock solution allowed to control the thickness of the fibrous aggregated morphologies for (S)-100-ET-PCD (Figure 8, panels a–f). Thus, the fibers with an average diameter ~ 76 nm (panel b) and 38–60 nm (panel c) transformed into 30–40 nm fibrous network (panel e) and ~ 12 –20 nm assemblies (panel f).

AFM inspection of other alkyne PCD series confirmed the general trend (Figures S26–S31) when stock solutions dilution resulted in diminishing the size of aggregated morphologies formed (e.g., “thick” fiber-like network at relatively high concentrations tend to transform into thin separated fibers). The ease with which polycarbodiimide thin film could be ruptured yielding “dewets” implies fairly weak association of polymer material with a substrate. These observations are consistent with a model developed for crater formation explaining such a defect as a result of the gradients in coating surface tension.^{72a}

In general, direct visualization of individual fibers seemed to be a challenging goal; however, using very low concentration provides an excellent opportunity to acquire images of isolated fibrillar aggregates.

Concentration series (Figure 9) performed on (S)-15-TRZ-85-Ph-PCD showed slightly different aggregation behavior upon dilution compared to the above-mentioned. While there is no evidence for the thin (~ 15 nm) separate fiber-like aggregates such as the ones seen in the panel d of Figure 1, the morphologies in new series are packed in a way that permits visualization of the curved bundles of fibers (Figure 9c,d,f). Spin coating from CHCl_3 stock generated curl-like assemblies that tend to become more separated one from another upon dilution (a–d and e, f series). Apparently, individual fibers (not connected into any kind of network or bundled) cannot be seen at relatively high concentration such as $C = 0.625$ mg/mL,

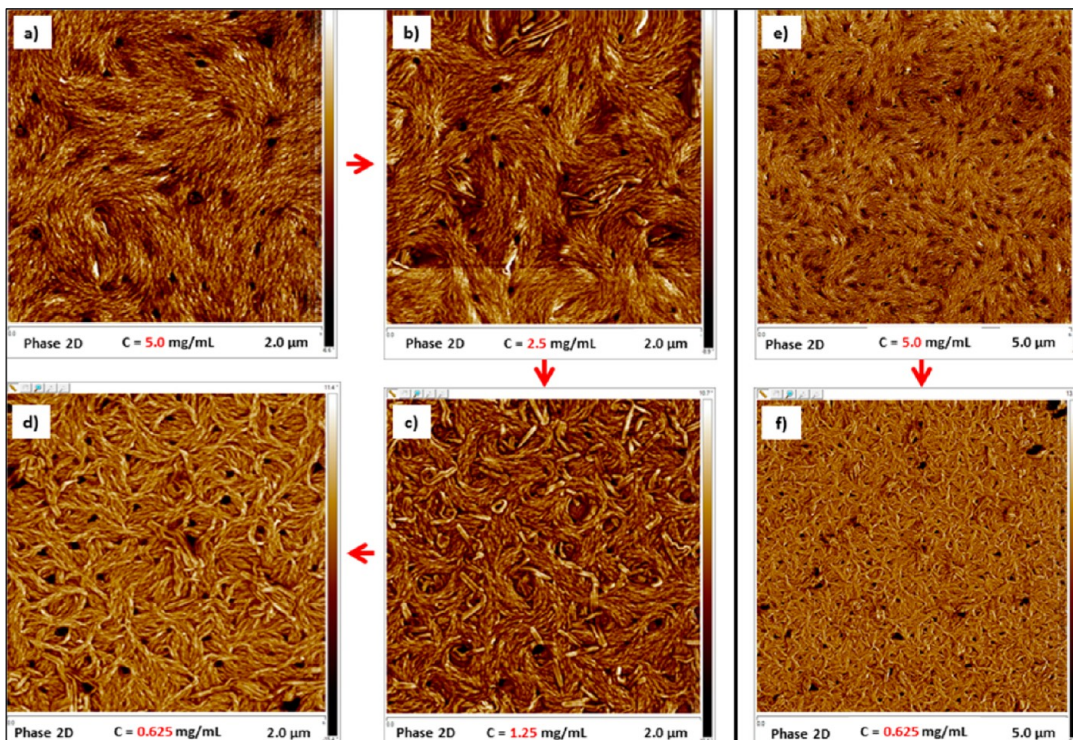


Figure 9. Phase AFM micrographs of (S)-15-TRZ-85-Ph-PCD. Morphological changes observed at dilution of the CHCl_3 stock solutions (spin-coated samples): 5.0 mg/mL (panels a, e); 2.5 mg/mL (panel b); 1.25 mg/mL (panel c); 0.625 mg/mL (panels d, f). Scan size = $2.0 \times 2.0 \mu\text{m}$ (panels a–d); $5.0 \times 5.0 \mu\text{m}$ (panels e, f).

implying that more dilute solutions are needed to prevent crystallization of individual polymer strands into supramolecular aggregates. Dimensions of bundled aggregates vary from ~ 25 to 43 nm (Figure 9d); however, the sample appears to be too concentrated for an accurate diameter analysis. Again, formation of these morphologies can be best explained by minimization of the unfavorable film/substrate contact as a result of thin film dewetting.

Direct Observation of Right- and Left-Handed Supramolecular Helical Structures. Short concentration series (Figure 10) were performed on selected PCDs ((S)-15-ET-85-Ph-, (S)-85-ET-15-Ph-, and (R)-85-ET-15-Ph-compositions) spin-coated either from THF or from the mixture of THF/EtOH (25% by volume) in order to visualize fibers/toroidal structures described earlier more distinctively. AFM inspection in light tapping mode displayed a great variety of highly ordered structures (fibrous networks, individual fibers, looped fibers, worm-like aggregates, toroidal structures) that believed to be arrays of tightly packed single helical chains (Figure 2S1–2S16). Thus, applying medium range concentrations ($C = 0.5$ – 1.0 mg/mL) for spin-coating technique allowed us to acquire very clear images of the fibrous aggregates with average width of fibers $\sim 70 \text{ nm}$ (Figure 10a–c and Figure 2S3). Unusual looped supramolecular constructs closely related to toroidal motifs can be observed in the panels d and e (Figure 10). More morphologies of this nature were deposited in the Supporting Information, Vol. 2 (Figures 2S6f, 2S7, 2S8, 2S9a,d,l, 2S10a–d, and 2S11). It seemed likely that some of these ring-like aggregates are indeed a part of fibrillar network (crystallized with adjacent fibers like images shown in panels d–f of Figure 10 with estimated “wall” thickness ~ 55 – 64 nm (Figure 2S7, 2S8, and 2S11); however, in very few cases we were able to detect isolated toroids of 241 nm in size (Figure 10i).

Notably, very distinct 8-number-shaped fiber could be observed in the panels g and h (Figure 10) with two small toroids embedded into the upper and lower parts of this architecture. Given the fact that the difference between experimentally observed looped fibers and toroids is not quite clear, we assume that different mechanisms/models should be applied to their description; however, this is not focus of the current work. The rest of images (Figure 10, lower panels j–l) demonstrated aggregation behaviors of (S)-15-ET-85-Ph-PCD depending on concentration. The major advantage of using relatively high concentration in this case (1.0 and 0.5 mg/mL) is ability to resolve fiber segments in short worm-like aggregates (panel j) and extensive fibrous networks (panels k and l) images. Further studies afforded high contrast images of individual fibers (Figure 11a,c) and even visualization of superhelical turns (Figure 11b,d,e and Figure 2S3) of both right- and left-handed screw senses. To our knowledge, this is the first direct observation of polycarbodiimides superhelical turns with pitch size varying from 71 to 119 nm . We infer that superhelical structures^{72b} are composed of a plenty of individual PCD-macromolecules assembled into the bundle. Magnified image of left-handed superhelical motif is depicted in panel e of Figure 11 (Figure 2S3). Interestingly, self-assembly of both left-handed (S)-PCDs (Figure 11) in thin film resulted in formation the helices having left and right screw senses; however, left-handedness seemed to be predominant for the morphologies shown. We assume that this is due to translation of chiral information from individual macromolecules level to their assemblies, so S-polycarbodiimides single molecules tend to form left-handed superstructures. Another possible explanation of this aggregation behavior involves “twisting during crystallization” phenomenon similar to the results reported^{72c}

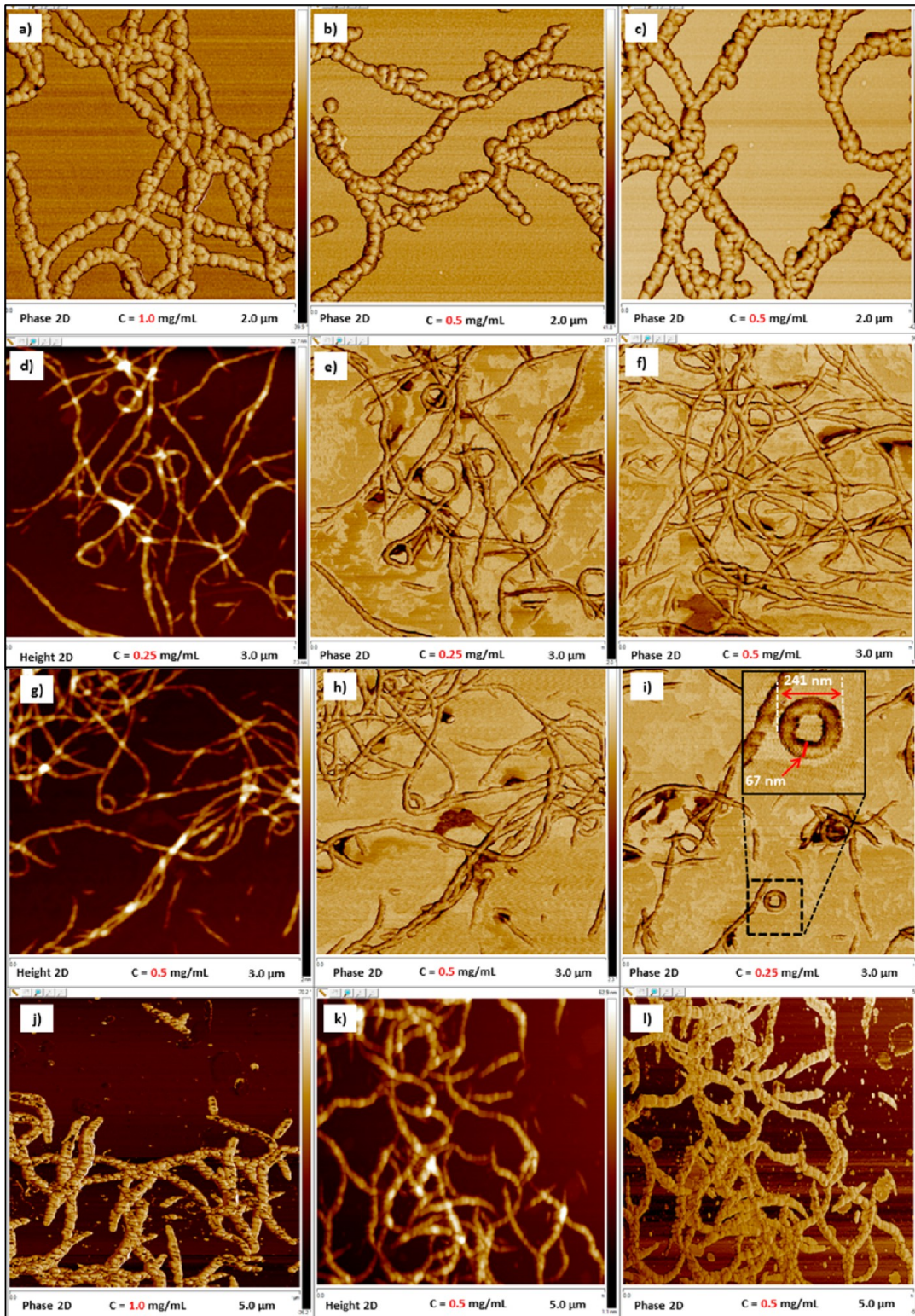


Figure 10. Phase and height AFM micrographs of (S)-85-ET-15-Ph-PCD (panels a–c, f) and (R)-85-ET-15-Ph-PCD (panels d, e, g–i), and (S)-15-ET-85-Ph-PCD (panels j–l). Scan size = $2.0 \times 2.0 \mu\text{m}$ (panels a–c); $3.0 \times 3.0 \mu\text{m}$ (panels d–i); $5.0 \times 5.0 \mu\text{m}$ (panels j–l).

when chiral character of the resulting supramolecular objects is imparted by crystallization process.

In general, comparing images from CHCl_3 and THF/EtOH (25%) series, we can infer that regardless of solvent system used PCDs molecules tend to form essentially the same packing motif with predominance of fibrous aggregates.

TEM and SEM Characterization. In order to corroborate our AFM morphological findings, representative alkyne and triazole PCDs were studied by electron microscopy techniques such as transmission electron microscopy (TEM) and scanning electron microscopy (SEM). A wide range of reported electron spectroscopy characterizations of elongated supramolecular species assembled from covalent polymers involves nanofibers

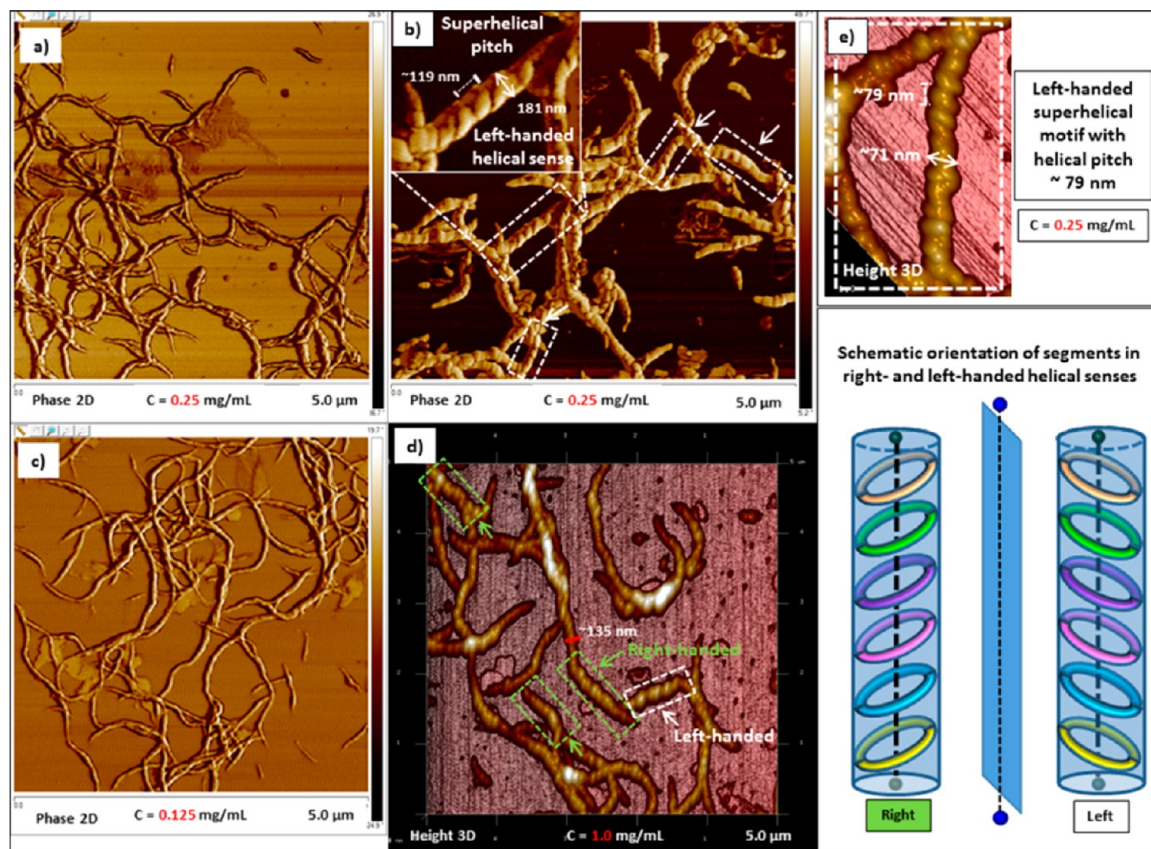


Figure 11. Phase and height AFM micrographs of (S)-15-ET-85-Ph-PCD (panels a–d) and (S)-85-ET-15-Ph-PCD (panel e). Scan size = $5.0 \times 5.0 \mu\text{m}$ (panels a–d).

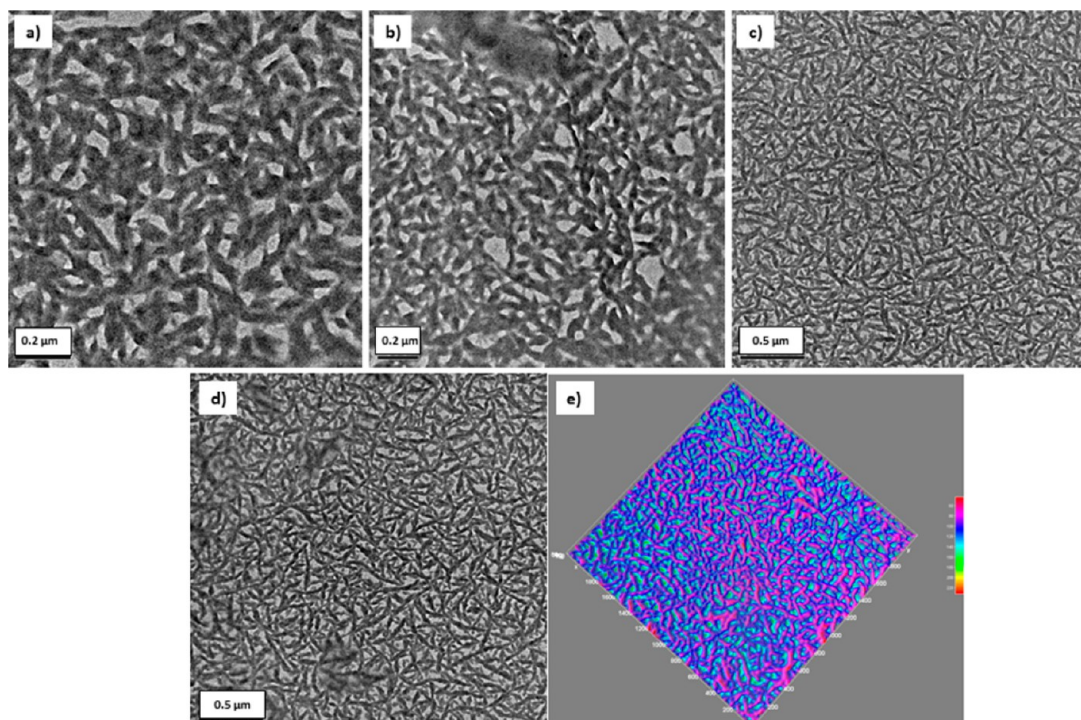


Figure 12. TEM micrographs of (S)-30-TRZ-70-Ph-PCD drop-cast from CHCl_3 ($C = 0.8 \text{ mg/mL}$) on carbon-coated copper grid (panels a, b); (R)-30-ET-70-Ph-PCD drop-cast from CHCl_3 ($C = 0.8 \text{ mg/mL}$), panels c–e. Scale bar = $0.2 \mu\text{m}$ (panels a, b); $0.5 \mu\text{m}$ (panels c–e); panel e represents ImageJ-processed micrograph 10d to enhance 3D perception of morphologies observed.

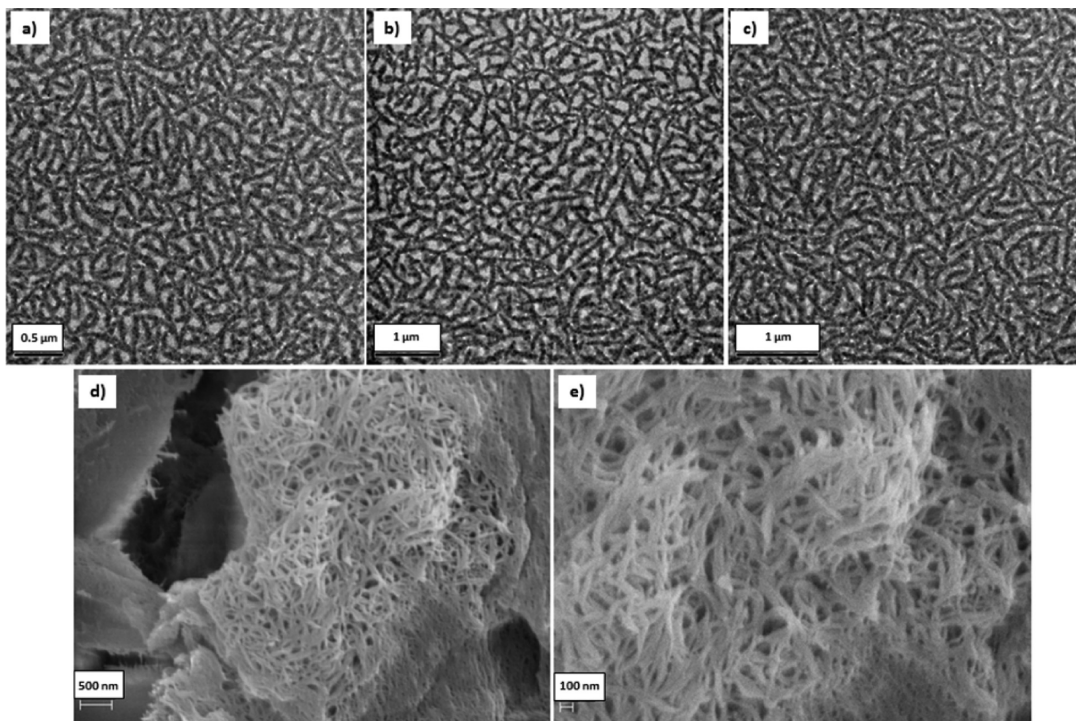


Figure 13. TEM micrographs of (R)-50-ET-50-Ph-PCD drop-cast from CHCl_3 ($C = 0.8 \text{ mg/mL}$) on carbon-coated copper grid (panels a–c); SEM micrographs of (S)-15-TRZ-85-Ph-PCD powder (panels d, e). Scale bar = $0.5 \mu\text{m}$ (panel a); $1.0 \mu\text{m}$ (panels b, c); 500 nm (panel d); 100 nm (panel e).

including bundled and branched ones,⁷³ lamellar structures,⁷⁴ core–shell nanofibers,⁷⁵ elongated nanoribbons, worm-like micelles,^{76,77} and submicron fibers.⁷⁸ Also, unusual rigid-rod nanostructures derived from dynamic polymer systems⁷⁹ should not be underestimated. TEM images (Figures 12 and 13, Figure S32) showed clear structural features resembling morphologies described above. Thus, (S)-30-TRZ-70-Ph-PCD (Figure 12a,b) and (R)-30-ET-70-Ph-PCD (Figure 12c–e) drop-cast on carbon-coated copper grid from dilute CHCl_3 solution revealed the formation of well-organized fiber-like networks (especially pronounced in panels c–e). More details on TEM-imaging could be found in the Supporting Information (Figure S32). We did not anticipate the visualization of exactly the same looking aggregates shown in AFM section; our goal in this study was to mimic thin film preparation as close as possible to the standard AFM technique. We realize that use of different substrates need of high vacuum may finally alter results compared to our AFM observations.

Unlike other specimen studied, (R)-50-ET-50-Ph-PCD provided slightly better visualization contrast of the network pattern (Figure 13a–c and Figure S32e,f), otherwise unremarkable changes. For all polymers inspected, the general appearance of networks imaged by TEM was found to be essentially identical.

Assessment of (S)-15-TRZ-85-Ph-PCD powder sample by SEM showed bent nanofibers organized into network (Figure 13d,e) with estimated fiber width ranging from ~ 31 to 61 nm and length $\sim 400 \text{ nm}$. Lower right panel (Figure 13e) showed the highest magnification of specimen that allows taking measurements of separate fibers (Figure S34). Additional SEM micrographs displaying fibrillary morphologies could be found in Figures S35 and S35-2. The powder sample was mounted on double-stick carbon tape and then coated with conductive Pd/Au film to minimize charge buildup and heating of the sample

by electron beam when running acquisition. The major challenge was, of course, thermal stability of organic polymer specimen exposed to e-beam. Nonfunctionalized PCDs are known to be fairly stable⁵² that was also confirmed by our studies. (TGA thermograms of (R)-15-TRZ-85-Ph- and (S)-15-TRZ-85-Ph-PCDs displayed in Figure S33 suggested that sample decomposition/weight loss occurred only at $T > 180^\circ\text{C}$. This ensures that polymer specimen would likely remain intact during SEM/TEM acquisitions without reorganizing itself into the different morphology.)

Bearing in mind that the nature of hydrophobic side chain/side chain interactions responsible for macromolecules communication in thin film and bulk is the same, we surmise that results obtained for crystalline sample might be further used for interpretation of the self-assembly in thin film. Overall, we have demonstrated that TEM and SEM techniques could be successfully applied to characterize independently fiber-like morphologies first discovered by TMAFM analysis.

Powder X-ray Diffraction Studies of Alkyne PCDs and Their Triazole Derivatives. Powder X-ray diffraction (pXRD) measurements of alkyne and triazole PCDs were carried out to assess the ability of macromolecules to crystallize with one another into network structure and to provide a model of such kind of interactions. In these studies, it was not possible to collect any meaningful data using polymer thin film samples spin-coated onto Si-wafer from dilute CHCl_3 stocks ($C < 1 \text{ mg/mL}$) which were used for AFM inspection; therefore, measurements were taken for specimen prepared from powder samples deposited on SiO_2 . In addition to that, we also investigated (R)-100-Ph-PCD ($C \sim 30 \text{ mg/mL}$) drop-cast onto Si-wafer. Figure 14 and Figure S36 show exemplary pXRD patterns of (S)-85-ET-15-Ph- and (R)-15-TRZ-85-Ph-PCDs. One noticeable peak is apparent at $\sim 7^\circ$ for all alkyne and triazole PCDs studied. It is uncertain to which particular

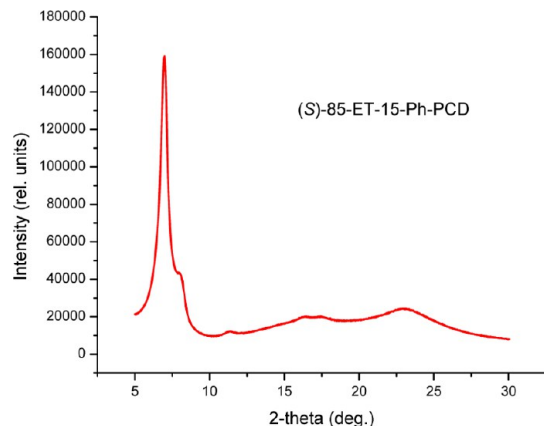


Figure 14. Powder X-ray diffraction pattern of (S)-85-ET-15-Ph-PCD.

component in composition this peak must be assigned to, since two blocks have chemically reasonable difference in structure (ethynyl group vs hydrogen atom), but seemingly exhibit very little difference in their X-ray diffraction properties (like all organic materials incorporated no heavy atoms and, therefore, diffracting weakly). Corresponding *d*-spacing values ($\sim 12 \text{ \AA}$) calculated from these diffraction angles are believed to be the distance between adjacent polymer helices in the crystal lattice which matches closely to the proposed model of dimeric bundle.

A small shoulder appeared at $\sim 8^\circ$ (2θ) in the diffraction profile may correspond to the second constituent in composition.

We speculate that the first order peak at 7° provides evidence for self-assembly in solid state and may result from lamellar stacking of macromolecular strands similar to the highly ordered block copolymers having poly(3-alkylthiophene) moiety.^{59,60,80} The second broad peak (or a group of overlapping peaks) at $2\theta \sim 20^\circ\text{--}23^\circ$ ($d \sim 4 \text{ \AA}$) is barely above the noise level and can potentially be attributed to the $\pi\text{--}\pi$ stacking interaction^{60,81a} of aromatic fragments (Tables S3 and S4) or lateral spacings between side groups within the layers formed by polymer main chains.^{81b} Detailed analysis and attribution of these higher order reflection peaks without additional spectral evidence would be presumptuous and misleading. Film XRD profile (Figure S36-2) recorded for (R)-100-Ph-PCD demonstrated essentially the same features observed for its respective powder analogue just with more pronounced broad peaks in the region from 15° to 25° corresponding to $\pi\text{--}\pi$ stacking.

Modeling of Side-Chain Interactions. Recently, dodecyl side-chain interdigititation was discovered for short-chain thiazolothiazole-thiophene copolymers.⁸² It was found that lamellar *d*-spacings values are indicative of vertically adjacent polymer backbones that are packed very closely. Another important observation was made for spin-coated and cast poly(3-hexylthiophene) film model structures⁸³ that display planarized and ordered segments of thiophene backbone decorated by *n*-hexyl side chains. In our case, *n*-hexyl groups appended to polycarbodiimide scaffold are believed to project toward each other yielding supramolecular stack with *d*-spacing $\sim 12 \text{ \AA}$ that correlates nicely with the distances between neighboring helices in proposed dimeric bundle model (Figure 15d). Optimized geometry for a singular polymer strand having left-handed helical array of *n*-C₆-pendants spinning around the polycarbodiimide backbone was calculated by using the 20-mer

model (Gaussian 09W, semiempirical AM1; Figure 15a,b) with a helical pitch $\sim 15.1 \text{ \AA}$ and the distance between centroids of adjacent phenyl rings ranging from 5.96 to 7.45 \AA . Depending on the nature of helical scaffold, the helical pitch may vary significantly. For example, the layer distance corresponding to helical pitch in 20-mer model of poly(*p*-*n*-hexyloxyphenylacetylenes)¹⁸ was calculated to be 3.4 \AA , whereas AFM measurements of poly(*m*-phenylene ethynylene)s³³ followed by XRD analysis and molecular mechanics calculations exhibited helical pitch of 1.03 nm in size. Additionally, the helical pitch, or the distance between identical places on neighboring helical turns, can fluctuate but estimated to be around 13.7 \AA for PCD macromolecules.³⁶ Panels a and c of Figure 15 depicted the diameter of the singular polymer strand ($\sim 15 \text{ \AA}$) with respect to the fully extended *n*-hexyl side chains (paraffin chain corona) and its respective heptamic bundle ($\sim 40 \text{ \AA}$). Taking into account that most fibers identifiable by the AFM technique have diameter around 50–100 nm, it seems possible that they are composed of dozens or even hundreds of individual macromolecules self-assembled into the bundled superstructures. Even very thin fibers/elongated morphologies displayed in panel d of Figure 2 and Figure S6b (R-15-TRZ-85-Ph-PCD spin-coated from CHCl₃ on HOPG substrate) likely represent bundles of individual macromolecules. Although semiempirical calculations may not adequately reflect the real polycarbodiimide backbone geometry, they generally comport with our XRD findings. Panel d showed a diagrammatic sketch of dimeric bundle assembled from individual helices as a result of hydrophobic side chain interactions with a distance between polymer strands evaluated to be around 12.5 \AA . The latter can be attributed to lamellar *d*-spacing ($\sim 12 \text{ \AA}$) found in PCDs.

Presumably, further aggregation of individual macromolecules as a result of the extensive self-assembly would lead to the formation of even more complex supramolecular bundles (e.g., trimers, tetramers, pentamers, etc.).

Of course, conclusive proof for interdigitation of individual polymer helices in supramolecular bundle arrays should require developing the robust method of crystallizing these macromolecular species to employ single crystal X-ray analysis. However, the difficulty in crystallizing organic polymers begins with having uniform material. Given the fact that controlled living polymerization of carbodiimide monomers⁵² always yields a wide range of molecular weights corresponding to the different length polymer chains, successful growing single crystals of these materials will probably be a significant challenge.

Admittedly, alignment of lateral chains relative to the normal of the unit cell plane in supramolecular bundles and their interpenetration ability to form interdigititation pattern remain a matter for speculation. Thus, MM optimizations performed for (PE)₁₂-*b*-(DMS)₁₅ chains⁸⁴ suggested that noninterdigitating motif for macromolecules is possible. Also, C₇H₁₅ side chains of the helical poly(*m*-phenylene) derivatives were found to be either slightly interdigitated or not interdigitated but separated to each other depending on phase (discotic or smectic).⁸⁵ That would definitely display some effect on interhelical separation in bundled superstructures; e.g., the distance between adjacent polymer strands in the bundle may be a subject to change depending on the length of chains and their ability to interlock with each other. We realize that model proposed is limited to alkyne PCDs only and may not be satisfactorily used to explain aggregation behavior of their triazole derivatives having much

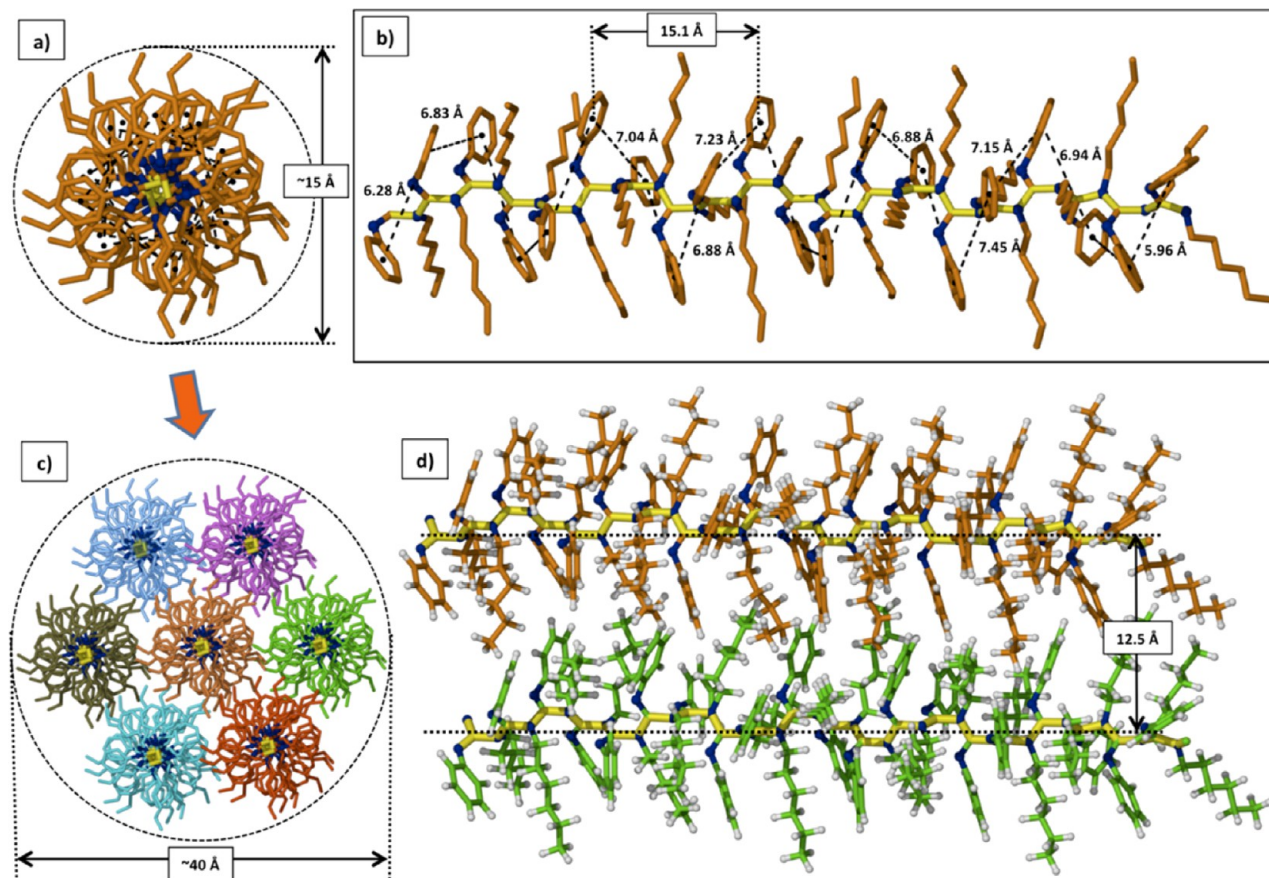


Figure 15. Calculated structure of left-handed (S)-100-Ph-PCD front view (panel a) and side view (panel b); schematic representation of heptameric assembly, front view (panel c); model of the dimeric bundle, side view (panel d), polycarbodiimide backbone is depicted in yellow.

more bulkier moieties appended to aromatic rings like shown in hypothetical model of (*R*)-50-TRZ-50-Ph-PCD (Figure S66), and therefore hydrophobic *n*-hexyl side chain interactions would likely play a less important role in communication of individual macromolecular strands.

Altogether, these results strongly suggest, but do not unambiguously prove, that self-assembly of such polycarbodiimides is mostly driven by hydrophobic side chain/side chain interactions.

CONCLUSIONS

In summary, it is reasonable to conclude that formation of fiber-like aggregates, ribbons, worm-like structures, fibrillar networks, looped fibers, toroids, and other elongated morphologies revealed by AFM may be associated at molecular level with the interdigitation of *n*-hexyl side chains protruding from polycarbodiimide backbone. Furthermore, interdigitation is influenced by alkyl side chain length as well as their ability to interlock. This implies that variations in side chain structures allow to tune hydrophobic interactions and hence control aggregation. Our goal in this work was to construct reasonable model addressing concerns on how individual macromolecular helices may communicate with each other aggregating into supramolecular bundled superstructures that could be visualized by AFM in the thin film. Importantly, TEM specimen prepared according to AFM protocol exhibited similarly looking cross-linking fibrillar motifs, thus providing independent evidence to AFM observations. Moreover, to prove the existence of fibrillar morphologies beyond the aggregation in

thin film, we inspected powder samples by both SEM and pXRD techniques showing results that support and complement AFM data. Also, AFM data strongly supported formation of superhelical motifs in specimens prepared from THF/EtOH (25%) solvent mixture. This important observation of both left- and right-handed superhelices is the first visual evidence of superhelical chiral induction made on polycarbodiimides. Extensive dilution series carried out for PCDs confirmed propensity of macromolecules to self-assemble into fibrillar aggregates at different concentrations thus providing a handy tool to control the thickness of nanofibers that might represent significant interest for potential technological applications. In general, these studies provide unique insights into aggregation behavior of the individual polycarbodiimide helices. In this context, it is remarkably important to reveal the underlying mechanisms of polycarbodiimides self-assembly at molecular level to further successfully manipulate and direct the organization of fascinating morphologies constructed thereof.

ASSOCIATED CONTENT

S Supporting Information

Figures S1–S66 and Figures 2S1–2S16; Tables S1–S4. The Supporting Information is available free of charge on the ACS Publications website at DOI: 10.1021/acs.macromol.5b00407.

AUTHOR INFORMATION

Corresponding Authors

*Ph +1 (215) 470-3581; e-mail oleg.kulikov.chem@gmail.com (O.V.K.).

*Ph +1 (972) 883-2416; e-mail Bruce.Novak@utdallas.edu (B.M.K.).

Notes

The authors declare no competing financial interest.

ACKNOWLEDGMENTS

Funding for this work was provided by the Faculty start-up fund from the University of Texas at Dallas (UTD) and the Endowed Chair for Excellence at UTD. We acknowledge Benjamin Batchelor, Dr. Sumudu Wijenayake, and Sahila Perananthan for assistance with GPC, TGA, and XRD. We gratefully acknowledge the NSF-MRI grant (CHE-1126177) used to purchase the Bruker Advance III 500 NMR instrument.

REFERENCES

- (1) Yashima, E.; Maeda, K.; Iida, H.; Furusho, Y.; Nagai, K. *Chem. Rev.* **2009**, *109*, 6102–6211.
- (2) Miyabe, T.; Hase, Y.; Iida, H.; Maeda, K.; Yashima, E. *Chirality* **2009**, *21*, 44–50.
- (3) Iida, H.; Iwahana, S.; Mizoguchi, T.; Yashima, E. *J. Am. Chem. Soc.* **2012**, *134*, 15103–15113.
- (4) Shimomura, K.; Ikai, T.; Kanoh, S.; Yashima, E.; Maeda, K. *Nat. Chem.* **2014**, *6*, 429–434.
- (5) Qi, S.; Iida, H.; Liu, L.; Irle, S.; Hu, W.; Yashima, E. *Angew. Chem., Int. Ed.* **2013**, *52*, 1049–1053.
- (6) Qi, T.; Deschrijver, T.; Huc, I. *Nat. Protoc.* **2013**, *8*, 693–708.
- (7) Sanchez-Garcia, D.; Kauffmann, B.; Kawanami, T.; Ihara, H.; Takafuji, M.; Delville, M.; Huc, I. *J. Am. Chem. Soc.* **2009**, *131*, 8642–8648.
- (8) Shang, J.; Gan, Q.; Dawson, S. J.; Rosu, F.; Jiang, H.; Ferrand, Y.; Huc, I. *Org. Lett.* **2014**, *16*, 4992–4995.
- (9) Baptiste, B.; Douat-Casassus, C.; Laxmi-Reddy, K.; Godde, F.; Huc, I. *J. Org. Chem.* **2010**, *75*, 7175–7185.
- (10) Kendhale, A. M.; Poniman, L.; Dong, Z.; Laxmi-Reddy, K.; Kauffmann, B.; Ferrand, Y.; Huc, I. *J. Org. Chem.* **2011**, *76*, 195–200.
- (11) Delsuc, N.; Massip, S.; Leger, J.; Kauffmann, B.; Huc, I. *J. Am. Chem. Soc.* **2011**, *133*, 3165–3172.
- (12) Ferrand, Y.; Kendhale, A. M.; Kauffmann, B.; Grelard, A.; Marie, C.; Blot, V.; Pipelier, M.; Dubreuil, D.; Huc, I. *J. Am. Chem. Soc.* **2010**, *132*, 7858–7859.
- (13) Ferrand, Y.; Chandramouli, N.; Kendhale, A. M.; Aube, C.; Kauffmann, B.; Grelard, A.; Laguerre, M.; Dubreuil, D.; Huc, I. *J. Am. Chem. Soc.* **2012**, *134*, 11282–11288.
- (14) Gan, Q.; Ferrand, Y.; Chandramouli, N.; Kauffmann, B.; Aube, C.; Dubreuil, D.; Huc, I. *J. Am. Chem. Soc.* **2012**, *134*, 15656–15659.
- (15) (a) Sanda, F.; Terada, K.; Masuda, T. *Macromolecules* **2005**, *38*, 8149–8154. (b) Akagi, K. *Chem. Rev.* **2009**, *109*, 5354–5401. (c) Liu, J.; Lam, J. W. Y.; Tang, B. Z. *Chem. Rev.* **2009**, *109*, 5799–5867.
- (16) Maeda, K.; Wakasone, S.; Shimomura, K.; Ikai, T.; Kanoh, S. *Macromolecules* **2014**, *47*, 6540–6546.
- (17) Ohsawa, S.; Sakurai, S.; Nagai, K.; Banno, M.; Maeda, K.; Kumaki, J.; Yashima, E. *J. Am. Chem. Soc.* **2011**, *133*, 108–114.
- (18) Motoshige, A.; Mawatari, Y.; Yoshida, Y.; Seki, C.; Matsuyama, H.; Tabata, M. *J. Polym. Sci., Part A: Polym. Chem.* **2012**, *50*, 3008–3015.
- (19) Percec, V.; Rudick, J. G.; Wagner, M.; Obata, M.; Mitchell, C. M.; Cho, W.; Magonov, S. N. *Macromolecules* **2006**, *39*, 7342–7351.
- (20) Tonelli, A. E. *Macromolecules* **1974**, *7*, 628–631.
- (21) Lifson, S.; Andreola, C.; Peterson, N. C.; Green, M. M. *J. Am. Chem. Soc.* **1989**, *111*, 8850–8858.
- (22) Troxell, T. C.; Scheraga, H. A. *Macromolecules* **1971**, *4*, 528–539.
- (23) Sugita, A.; Yamashita, Y.; Tasaka, S. *J. Polym. Sci., Part B: Polym. Phys.* **2005**, *43*, 3093–3099.
- (24) Ahn, J.; Shin, Y.; Kim, S.; Lee, J. *Polymer* **2003**, *44*, 3847–3854.
- (25) Green, M. M.; Khatri, C. A.; Reidy, M. P.; Levon, K. *Macromolecules* **1993**, *26*, 4723–4725.
- (26) Kikuchi, M.; Lien, L. T. N.; Narumi, A.; Jinbo, Y.; Izumi, Y.; Nagai, K.; Kawaguchi, S. *Macromolecules* **2008**, *41*, 6564–6572.
- (27) Rubingh, D. N.; Yu, H. *Macromolecules* **1976**, *9*, 681–685.
- (28) Goodman, M.; Chen, S. *Macromolecules* **1970**, *3*, 398–402.
- (29) Maeda, K.; Okamoto, Y. *Macromolecules* **1998**, *31*, 1046–1052.
- (30) Shibaev, P. V.; Tang, K.; Genack, A. Z.; Kopp, V.; Green, M. M. *Macromolecules* **2002**, *35*, 3022–3025.
- (31) Muller, M.; Zentel, R. *Macromolecules* **1994**, *27*, 4404–4406.
- (32) (a) Aharoni, S. M.; Walsh, E. K. *Macromolecules* **1979**, *12*, 271–276. (b) Aharoni, S. M. *Polymer* **1980**, *21*, 21–30.
- (33) Banno, M.; Yamaguchi, T.; Nagai, K.; Kaiser, C.; Hecht, S.; Yashima, E. *J. Am. Chem. Soc.* **2012**, *134*, 8718–8728.
- (34) (a) Kajitani, T.; Onouchi, H.; Sakurai, S.; Nagai, K.; Okoshi, K.; Onitsuka, K.; Yashima, E. *J. Am. Chem. Soc.* **2011**, *133*, 9156–9159. (b) Jiang, Z.; Xue, Y.; Chen, J.; Yu, Z.; Liu, N.; Yin, J.; Zhu, Y.; Wu, Z. *Macromolecules* **2015**, *48*, 81–89.
- (35) Zhu, Y.; Yin, T.; Li, X.; Su, M.; Xue, Y.; Yu, Z.; Liu, N.; Yin, J.; Wu, Z. *Macromolecules* **2014**, *47*, 7021–7029.
- (36) Kennemur, J. G.; Novak, B. M. *Polymer* **2011**, *52*, 1693–1710.
- (37) (a) Kennemur, J. G.; Novak, B. M. *Isr. J. Chem.* **2011**, *51*, 1041–1051. (b) Budhathoki-Uprety, J.; Jena, P. V.; Roxbury, D.; Heller, D. A. *J. Am. Chem. Soc.* **2014**, *136*, 15545–15550.
- (38) Goodwin, A.; Novak, B. M. *Macromolecules* **1994**, *27*, 5520–5522.
- (39) Arnold, L.; Marx, A.; Thiele, C. M.; Reggelin, M. *Chem.—Eur. J.* **2010**, *16*, 10342–10346.
- (40) Kennemur, J. G.; Clark, J. B., IV; Tian, G.; Novak, B. M. *Macromolecules* **2010**, *43*, 1867–1873.
- (41) Tang, H.; Boyle, P. D.; Novak, B. M. *J. Am. Chem. Soc.* **2005**, *127*, 2136–2142.
- (42) Reuther, J. F.; Novak, B. M. *J. Am. Chem. Soc.* **2013**, *135*, 19292–19303.
- (43) Merten, C.; Reuther, J. F.; DeSousa, J. D.; Novak, B. M. *Phys. Chem. Chem. Phys.* **2014**, *16*, 11456–11460.
- (44) Xue, Q.; Kimura, T.; Fukuda, T.; Shimada, S.; Matsuda, H. *Liq. Cryst.* **2004**, *31*, 137–143.
- (45) Kim, J.; Novak, B. M.; Waddon, A. *J. Macromolecules* **2004**, *37*, 8286–8292.
- (46) Budhathoki-Uprety, J.; Peng, L.; Melander, C.; Novak, B. M. *ACS Macro Lett.* **2012**, *1*, 370–374.
- (47) Liu, C.; Lin, C.; Kuo, C.; Lin, S.; Chen, W. *Prog. Polym. Sci.* **2011**, *36*, 603–637.
- (48) De Cuendias, A.; Hiorns, R. C.; Cloutet, E.; Vignau, L.; Cramail, H. *Polym. Int.* **2010**, *59*, 1452–1476.
- (49) Poser, S.; Fischer, H.; Arnold, M. *Prog. Polym. Sci.* **1998**, *23*, 1337–1379.
- (50) Zhang, J.; Chen, X.; Wei, H.; Wan, X. *Chem. Soc. Rev.* **2013**, *42*, 9127–9154.
- (51) Olsen, B. D.; Segalman, R. A. *Mater. Sci. Eng., R* **2008**, *62*, 37–66.
- (52) Reuther, J. F.; Bhatt, M. P.; Tian, G.; Batchelor, B. L.; Campos, R.; Novak, B. M. *Macromolecules* **2014**, *47*, 4587–4595.
- (53) Leclere, P.; Surin, M.; Viville, P.; Lazzaroni, R.; Kilbinger, A. F. M.; Henze, O.; Feast, W. J.; Cavallini, M.; Biscarini, F.; Schenning, A. P. H. J.; Meijer, E. W. *Chem. Mater.* **2004**, *16*, 4452–4466.
- (54) Leclere, P.; Surin, M.; Jonkheijm, P.; Henze, O.; Schenning, A. P. H. J.; Biscarini, F.; Grimsdale, A. C.; Feast, W. J.; Meijer, E. W.; Mullen, K.; Bredas, J. L.; Lazzaroni, R. *Eur. Polym. J.* **2004**, *40*, 885–892.
- (55) Budhathoki-Uprety, J.; Reuther, J. F.; Novak, B. M. *Macromolecules* **2012**, *45*, 8155–8165.
- (56) Budhathoki-Uprety, J.; Novak, B. M. *Macromolecules* **2011**, *44*, 5947–5954.
- (57) Barkey, N. M.; Tafreshi, N. K.; Josan, J. S.; De Silva, C. R.; Sill, K. N.; Hruby, V. J.; Gillies, R. J.; Morse, D. L.; Vagner, J. *Med. Chem.* **2011**, *54*, 8078–8084.
- (58) Iovu, M. C.; Craley, C. R.; Jeffries-EL, M.; Krankowski, A. B.; Zhang, R.; Kowalewski, T.; McCullough, R. D. *Macromolecules* **2007**, *40*, 4733–4735.

- (59) Bhatt, M. P.; Sista, P.; Hao, J.; Hundt, N.; Biewer, M. C.; Stefan, M. C. *Langmuir* **2012**, *28*, 12762–12770.
- (60) Bhatt, M. P.; Huynh, M. K.; Sista, P.; Nguyen, H. Q.; Stefan, M. C. *J. Polym. Sci., Part A: Polym. Chem.* **2012**, *S0*, 3086–3094.
- (61) Alemsegued, M. G.; Gowrisanker, S.; Servello, J.; Stefan, M. C. *Macromol. Chem. Phys.* **2009**, *210*, 2007–2014.
- (62) Alemsegued, M. G.; Servello, J.; Hundt, N.; Sista, P.; Biewer, M. C.; Stefan, M. C. *Macromol. Chem. Phys.* **2010**, *211*, 1291–1297.
- (63) Hundt, N.; Hoang, Q.; Nguyen, H.; Sista, P.; Hao, J.; Servello, J.; Palaniappan, K.; Alemsegued, M.; Biewer, M. C.; Stefan, M. C. *Macromol. Rapid Commun.* **2011**, *32*, 302–308.
- (64) Hundt, N.; Palaniappan, K.; Sista, P.; Murphy, J. W.; Hao, J.; Nguyen, H.; Stein, E.; Biewer, M. C.; Gnade, B. E.; Stefan, M. C. *Polym. Chem.* **2010**, *1*, 1624–1632.
- (65) Tang, H.; Garland, E. R.; Novak, B. M.; He, J.; Polavarapu, P. L.; Sun, F. C.; Sheiko, S. S. *Macromolecules* **2007**, *40*, 3575–3580.
- (66) Cheng, C.; Huang, Y.; Tang, R.; Chen, E.; Xi, F. *Macromolecules* **2005**, *38*, 3044–3047.
- (67) Pochan, D. J.; Chen, Z.; Cui, H.; Hales, K.; Qi, K.; Wooley, K. L. *Science* **2004**, *306*, 94–97.
- (68) Muller-Buschbaum, P.; Bauer, E.; Wunnicke, O.; Stamm, M. J. *Phys.: Condens. Matter* **2005**, *17*, S363–S386.
- (69) Muller-Buschbaum, P.; Bauer, E.; Maurer, E.; Schlogl, K.; Roth, S. V.; Gehrke, R. *Appl. Phys. Lett.* **2006**, *88*, 083114–3.
- (70) Schwartz, L. W.; Roy, R. V.; Eley, R. R.; Petrush, S. *J. Colloid Interface Sci.* **2001**, *234*, 363–374.
- (71) Reiter, G. *Langmuir* **1993**, *9*, 1344–1351.
- (72) (a) Evans, P. L.; Schwartz, L. W.; Roy, R. V. *J. Colloid Interface Sci.* **2000**, *227*, 191–205. (b) Cai, C.; Lin, J.; Chen, T.; Wang, X.; Lin, S. *Chem. Commun.* **2009**, 2709–2711. (c) Rosenthal, M.; Bar, J.; Burghammer, M.; Ivanov, D. A. *Angew. Chem., Int. Ed.* **2011**, *50*, 8881–8885.
- (73) Kamps, A. C.; Fryd, M.; Park, S. *ACS Nano* **2012**, *6*, 2844–2852.
- (74) Olsen, B. D.; Segalman, R. A. *Macromolecules* **2005**, *38*, 10127–10137.
- (75) Kapllani, A.; Dillard, C.; Washington, K. E.; Biewer, M. C.; Stefan, M. C.; Kalra, V. *Macromol. Mater. Eng.* **2014**, *299*, 1484–1493.
- (76) Shen, J.; Chen, C.; Fu, W.; Shi, L.; Li, Z. *Langmuir* **2013**, *29*, 6271–6278.
- (77) Thio, Y. S.; Wu, J.; Bates, F. S. *Macromolecules* **2006**, *39*, 7187–7189.
- (78) Qian, L.; Willneff, E.; Zhang, H. *Chem. Commun.* **2009**, 3946–3948.
- (79) Folmer-Andersen, J. F.; Buhler, E.; Candau, S.; Joulie, S.; Schmutz, M.; Lehn, J. M. *Polym. Int.* **2010**, *59*, 1477–1491.
- (80) Bhatt, M. P.; Du, J.; Rainbolt, E. A.; Pathiranage, T. M. S. K.; Huang, P.; Reuther, J. F.; Novak, B. M.; Biewer, M. C.; Stefan, M. C. *J. Mater. Chem. A* **2014**, *2*, 16148–16156.
- (81) (a) Thompson, C. M.; Li, F.; Smaldone, R. A. *Chem. Commun.* **2014**, 6171–6173. (b) Kim, J.; Novak, B. M.; Waddon, A. J. *Macromolecules* **2004**, *37*, 1660–1662.
- (82) Osaka, I.; Zhang, R.; Sauve, G.; Smilgies, D.; Kowalewski, T.; McCullough, R. D. *J. Am. Chem. Soc.* **2009**, *131*, 2521–2529.
- (83) Kobashi, M.; Takeuchi, H. *Macromolecules* **1998**, *31*, 7273–7278.
- (84) Leclerc, P.; Hennebicq, E.; Calderone, A.; Brocorens, P.; Grimsdale, A. C.; Mullen, K.; Bredas, J. L.; Lazzaroni, R. *Prog. Polym. Sci.* **2003**, *28*, 55–81.
- (85) Suda, K.; Akagi, K. *Macromolecules* **2011**, *44*, 9473–9488.